Mon. Not. R. Astron. Soc. **376,** 1301–1316 (2007) doi:10.1111/j.1365-2966.2007.11527.x

ESC observations of SN 2005cf – I. Photometric evolution of a normal Type Ia supernova

A. Pastorello,[1,2]★ S. Taubenberger,[1] N. Elias-Rosa,[1,3,4] P. A. Mazzali,[1,5] G. Pignata,[6] E. Cappellaro,[3] G. Garavini,[7] S. Nobili,[7] G. C. Anupama,[8] D. D. R. Bayliss,[9] S. Benetti,[3] F. Bufano,[3,10] N. K. Chakradhari,[8] R. Kotak,[11] A. Goobar,[7] H. Navasardyan,[3] F. Patat,[11] D. K. Sahu,[8] M. Salvo,[9] B. P. Schmidt,[9] V. Stanishev,[7] M. Turatto[3] and W. Hillebrandt[1]

[1]*Max-Planck-Institut für Astrophysik, Karl-Schwarzschild-Str. 1, D-85741 Garching bei München, Germany*
[2]*Astrophysics Research Centre, School of Mathematics and Physics, Queen's University Belfast, Belfast BT7 1NN*
[3]*INAF Osservatorio Astronomico di Padova, Vicolo dell'Osservatorio 5, I-35122 Padova, Italy*
[4]*Universidad de La Laguna, Av. Astrofísico Francisco Sánchez s/n, E-38206 La Laguna, Tenerife, Spain*
[5]*INAF Osservatorio Astronomico di Trieste, Via Tiepolo 11, I-34131 Trieste, Italy*
[6]*Departamento de Astronomía y Astrofísica, Pontificia Universidad Católica de Chile, Casilla 306, Santiago 22, Chile*
[7]*Department of Physics, Stockholm University, AlbaNova University Centre, SE-10691 Stockholm, Sweden*
[8]*Indian Institute of Astrophysics, Koramangala, Bangalore 560 034, India*
[9]*Research School of Astronomy and Astrophysics, Australian National University, Cotter Road, Weston Creek, ACT 2611, Australia*
[10]*Dipartimento di Astronomia, Università di Padova, Vicolo dell'Osservatorio 2, I-35122 Padova, Italy*
[11]*European Southern Observatory (ESO), Karl-Schwarzschild-Str. 2, D-85748 Garching bei München, Germany*

Accepted 2007 January 19; Received 2007 January 17; in original form 2006 April 28

ABSTRACT

We present early-time optical and near-infrared photometry of supernova (SN) 2005cf. The observations, spanning a period from about 12 d before to 3 months after maximum, have been obtained through the coordination of observational efforts of various nodes of the European Supernova Collaboration and including data obtained at the 2-m Himalayan *Chandra* Telescope. From the observed light curve we deduce that SN 2005cf is a fairly typical SN Ia with a post-maximum decline [$\Delta m_{15}(B)_{\rm true} = 1.12$] close to the average value and a normal luminosity of $M_{B,\rm max} = -19.39 \pm 0.33$. Models of the bolometric light curve suggest a synthesized ^{56}Ni mass of about 0.7 $M_{\odot}$. The negligible host galaxy interstellar extinction and its proximity make SN 2005cf a good Type Ia SN template.

Key words: supernovae: general – supernovae: individual: SN 2005cf – supernovae: individual: SN 1992al – supernovae: individual: SN 2001el – galaxies: individual: MCG-01-39-003 – galaxies: individual: NGC 5917.

1 INTRODUCTION

Type Ia supernovae (SNe Ia) have been extensively studied in recent years for their important cosmological implications. They are considered to be powerful distance indicators because they combine a high luminosity with relatively homogeneous physical properties. Moreover, observations of high-redshift SNe Ia have provided the clue for discovering the presence of a previously undetected cosmological component with negative pressure, labelled 'dark energy', and responsible of the accelerated expansion of the Universe (see Astier et al. 2006, and references therein).

Thanks to the collection of a larger and larger compendium of new data (e.g. Hamuy et al. 1996; Riess et al. 1999a; Jha et al. 2006), an unexpected variety in the observed characteristics of SNe Ia has been shown to exist, and it is only using empirical relations between luminosity and distance-independent parameters, for example, the shape of the light curve (see e.g. Phillips et al. 1993), that SNe Ia can be used as standardizable candles.

Actually Benetti et al. (2005) have recently shown that a one-parameter description of SNe Ia does not account for the observed variety of these objects. In order to understand the physical reasons that cause the intrinsic differences in Type Ia SNe properties, we need to improve the statistics by studying in detail a larger number of nearby objects. There are considerable advantages in analysing nearby SNe: one can obtain higher signal-to-noise ratio

★E-mail: pasto@mpa-garching.mpg.de

(S/N) data, and these SNe can be observed for a longer time after the explosion, providing more information on the evolution during the nebular phase. Moreover, due to their proximity, the host galaxies are frequently monitored by automated professional SN searches and/or individual amateur astronomers. This significantly increases the probability of discovering very young SNe Ia, allowing the study of these objects at the earlier phases after the explosion.

In order to constrain the explosion and progenitor models, excellent-quality data of a significant sample of nearby SNe Ia is necessary. To this end, a large consortium of groups, comprising both observational and modelling expertise has been formed (European Supernova Collaboration, ESC) as part of a European Research Training Network.[1]

To date, we obtained high-quality data for about 15 nearby SNe Ia. Analyses of individual SNe include SN 2002bo (Benetti et al. 2004), SN 2002er (Pignata et al. 2004; Kotak et al. 2005), SN 2002dj (Pignata et al., in preparation), SN 2003cg (Elias-Rosa et al. 2006), SN 2003du (Stanishev et al. 2007), SN 2003gs (Kotak et al., in preparation), SN 2003kf (Salvo et al., in preparation), SN 2004dt (Altavilla et al., in preparation) and SN 2004eo (Pastorello et al. 2007). Statistical analysis of samples of SNe Ia, including those followed by the ESC were performed by Benetti et al. (2005), Mazzali et al. (2005) and Hachinger, Mazzali & Benetti (2006).

The proximity of SN 2005cf and its discovery almost two weeks before the *B*-band maximum (see below) made it an ideal target for the ESC. Immediately following the discovery announcement, we started an intensive photometric and spectroscopic monitoring campaign, which covered the SN evolution over a period of about 100 d from the discovery. This is the first of two papers where ESC data of SN 2005cf are presented. This work is devoted to study the early time optical and IR photometric observations of SN 2005cf, while spectroscopic data will be presented in a forthcoming paper (Garavini et al., 2007).

The layout of this paper is as follows. In Section 2 the ESC observations of SN 2005cf will be presented, including a description of the data reduction techniques. In Section 3 the light curves of SN 2005cf will be displayed and analysed. In Section 4 we derive the main parameters of the SN using empirical relations from literature, while in Section 5 additional properties are inferred from light-curve modelling. We conclude the paper with a summary (Section 6).

2 OBSERVATIONS

2.1 SN 2005cf and the host galaxy

SN 2005cf was located close to the tidal bridge between two galaxies. It is known that the interaction between galaxies and/or galaxy activity phenomena may enhance the rate of star formation. As a consequence the rate of SNe in such galaxies is expected to increase. Although this scenario should favour mainly core-collapse SNe descending from short-lived progenitors, it could also increase the number of progenitors of SNe Ia with respect to the genuinely old stellar population (Della Valle & Livio 1994). Indeed Smirnov & Tsvetkov (1981) found indications of enhanced production of SNe of all types in interacting galaxy systems and Navasardyan et al. (2001) obtained a similar result in interacting pairs. More recently Della Valle et al. (2005) found evidence of an enhanced rate of SNe Ia in radio-loud galaxies, probably due to repeated episodes of interaction and/or merging. However, in general, the location of SN explosions does not seem to coincide with regions of strong interaction in the galaxies (Navasardyan et al. 2001), and the discovery of SNe in tidal tails remains an exceptional event (Petrosian & Turatto 1995). This makes SN 2005cf a very interesting case.

[1] http://www.mpa-garching.mpg.de/~rtn/

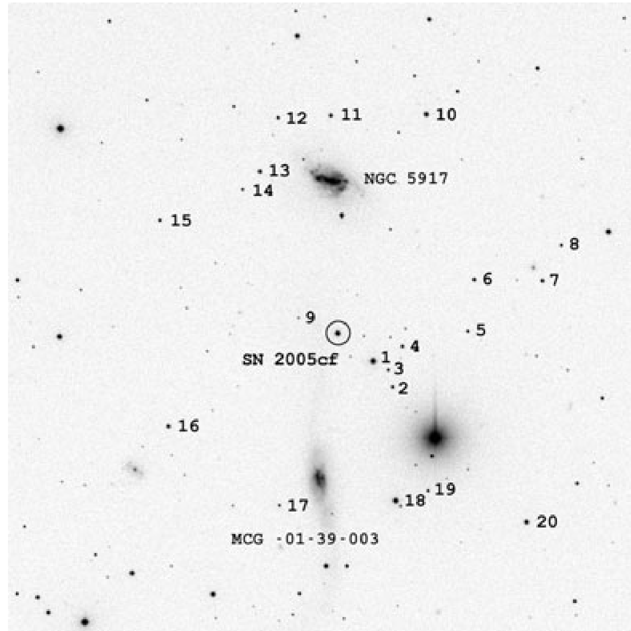

Figure 1. SN 2005cf in MCG-01-39-003: *B*-band image obtained on 2005 July 1 with the 2.2-m telescope of Calar Alto equipped with CAFOS. The field of view is 9 × 9 arcmin^2. The sequence stars of Table 2 are labelled with numbers. The galaxy below the SN in the image is MCG-01-39-003, the upper one is NGC 5917. North is up, east is to the left-hand side.

SN 2005cf was discovered by H. Pugh and W. Li with the KAIT telescope on May 28.36 UT when it was at magnitude 16.4 (Puckett et al. 2005). Puckett et al. (2005) also report that nothing was visible on May 25.37 UT to a limiting magnitude of 18.5. The coordinates of SN 2005cf are $\alpha = 15^h21^m32^s.21$ and $\delta = -07^\circ24'47''.5$ (J2000). The object is located 15.7 arcsec west and 123 arcsec north of the centre of MCG-01-39-003 (Fig. 1), a peculiar S0 galaxy [source NASA/IPAC Extragalactic Database (NED)].

SN 2005cf lies in proximity of a luminous bridge connecting MCG-01-39-003 with the Sb galaxy MCG-01-39-002 (also known as NGC 5917, see Fig. 1). This makes the association to one or the other galaxy uncertain. We will assume that SN 2005cf exploded in MCG-01-39-003, in agreement with Puckett et al. (2005), remarking that such assumption has no significant effect on the overall SN properties. Basic information on SN 2005cf, its host galaxy and the interacting companion is listed in Table 1.

Modjaz et al. (2005) obtained a spectrum on May 31.22 UT with the Whipple Observatory 1.5-m telescope (+FAST) and classified the new object as a young (more than 10 d before maximum light) Type Ia SN. This gave the main motivation for the activation of the follow-up campaign by the ESC.

2.2 ESC observations

We have obtained more than 360 optical data points, covering about 60 nights, from about 12 d before the *B*-band maximum to approximately 3 months after. In addition, near-infrared (NIR) observations have been performed in five selected epochs. Observations at late phases will be presented in a forthcoming paper.

Table 1. Main parameters for SN 2005cf, the host galaxy MCG-01-39-003 and the interacting companion NGC 5917.

	SN 2005cf	
α (J2000.0)	$15^h21^m32.21$	1
δ (J2000.0)	$-07°24'47''.5$	1
Offset galaxy–SN[a]	15.7 arcsec W, 123 arcsec N	1
SN Type	Ia	2
$E(B-V)_{\rm host}$	0	3
$E(B-V)_{\rm Gal}$	0.097	4
Discovery date (UT)	2005 May 28.36	1
Discovery JD	245 3518.86	1
Discovery magnitude	16.4	1
Pre-discovery limit epoch (UT)	2005 May 25.37	1
Pre-discovery limit magnitude	18.5	1
JD($B_{\rm max}$)	245 3534.0	3
$B_{\rm max}$	13.54	3
$M_{B,\rm max}(\mu)$	−19.39	3
$\Delta m_{15}(B)_{\rm true}$	1.12	3
s^{-1}	0.99	3
ΔC_{12}	0.355	3
t_r	18.6	3
$M(^{56}$Ni)	0.7 $M_\odot$	3
	MCG-01-39-003	
PGC name	PGC 054817	5
Galaxy type	S0 pec	5
α (J2000.0)	$15^h21^m33^s.29$	5
δ (J2000.0)	$-07°26'52''.38$	5
$B_{\rm tot}$	14.75 ± 0.43	6
D	1.4 × 0.7 arcmin^2	5
$v_{\rm Vir}$	1977 km s^{-1}	6
v_{3k}	2114 km s^{-1}	6
μ	32.51	3
$E(B-V)_{\rm Gal}$	0.098	4
	MCG-01-39-002 (NGC 5917)	
PGC name	PGC 054809	5
Galaxy type	Sb pec	5
α (J2000.0)	$15^h21^m32^s.57$	5
δ (J2000.0)	$-07°22'37''.8$	5
$B_{\rm tot}$	13.81 ± 0.50	6
D	1.5 × 0.9 arcmin^2	5
$v_{\rm Vir}$	1944 km s^{-1}	6
v_{3k}	2080 km s^{-1}	6
μ	32.51	3
$E(B-V)_{\rm Gal}$	0.095	4

[a]We assume MCG-01-39-003 as host galaxy.
Notes: 1 = Puckett et al. (2005); 2 = Modjaz et al. (2005); 3 = this paper; 4 = Schlegel et al. (1998); 5 = NED (http://nedwww.ipac.caltech.edu); 6 = LEDA (http://leda.univ-lyon1.fr).

During the follow-up, eight different instruments have been used for the optical and two for the NIR observations:

(i) the 40-in. telescope at the Siding Spring Observatory (Australia) with a Wide Field Camera (eight 2048 × 4096 CCDs, with pixel scale of 0.375 arcsec pixel^{-1}) and standard broad-band Bessell filters B, V, R, I;

(ii) the 3.58-m Italian Telescopio Nazionale Galileo (TNG) at the Observatorio de los Muchachos in La Palma (Canary Islands, Spain), equipped with DOLORES and a Loral thinned and back-illuminated 2048 × 2048 detector, with scale 0.275 arcsec pixel^{-1}, yielding a field of view of about 9.4 × 9.4 arcmin^2. We used the U, B, V Johnson and R, I Cousins filters (with TNG identification numbers 1, 10, 11, 12, 13, respectively);

(iii) the 2.5-m Nordic Optical Telescope in La Palma equipped with ALFOSC (with an E2V 2048 × 2048 CCD of 0.19 arcsec pixel^{-1}) and a set of U, B, V, R Bessell filters (with NOT identification numbers 7, 74, 75, 76, respectively) and an interference i-band filter (number 12);

(iv) the 2.3-m telescope in Siding Spring, equipped with the E2V 2048 × 2048 imager, with pixel scale of 0.19 arcsec pixel^{-1} and standard broad-band Bessell filters U, B, V, R, I;

(v) the Mercator 1.2-m Telescope in La Palma, equipped with a 2048 × 2048 CCD camera (MEROPE) having a field of view of 6.5 × 6.5 arcmin^2 and a resolution of about 0.19 arcsec pixel^{-1}. We used U, B, V, R, I filters (with identification codes UG, BG, VG, RG and IC, respectively);

(vi) the 2.2-m telescope of Calar Alto (Spain) equipped with CAFOS and a SITe 2048 × 2048 CCD, 0.53 arcsec pixel^{-1}; the filters available were the U, B, V, R, I Johnson (labelled as 370/47b, 451/73, 534/97b, 641/158, 850/150b, respectively);

(vii) the Copernico 1.82-m Telescope of Mt Ekar (Asiago, Italy); equipped with AFOSC, a TEKTRONIX 1024 × 1024 thinned CCD (0.47 arcsec pixel^{-1}) and a set of B, V, R Bessell and the i Gunn filters;

(viii) the ESO/MPI 2.2-m Telescope in La Silla (Chile), with a wide field mosaic of eight 2048 × 4096 CCDs (0.24 arcsec pixel^{-1}) and a total field of view of 34 × 33 arcmin^2. We used the broad-band filters U (labelled as ESO877), B (ESO878), V (ESO843), Cousins Rc (ESO844) and EIS I (ESO879);

(ix) the TNG equipped with the Near-Infrared Camera Spectrometer (NICS) with a HgCdTe Hawaii 1024 × 1024 array (field of view 4.2 × 4.2 arcmin^2, scale 0.25 arcsec pixel^{-1}); the filters used in the observations were J, H, K'.

(x) the 3.5-m telescope in Calar Alto with Omega-Cass, having a Rockwell 1024 × 1024 HgCdTe Hawaii array with pixel scale 0.2 arcsec pixel^{-1} and J, H, K' filters.

In this paper we also included the data from Anupama et al. (in preparation) obtained using the 2-m Himalayan *Chandra* Telescope (HCT) of the Indian Astronomical Observatory (IAO), Hanle (India), equipped with the Himalaya Faint Object Spectrograph Camera (HFOSC), with a SITe 2048 × 4096 CCD (pixel scale 0.296 arcsec pixel^{-1}), with a central region (2048 × 2048 pixels) used for imaging and covering a field of view of 10 × 10 arcmin^2. Standard Bessell U, B, V, R, I filters were used.

The U, B, V, R, I transmission curves for all optical instrumental configurations used during the follow-up of SN 2005cf are shown in Fig. 3, and compared with the standard Johnson–Cousins passbands (Bessell 1990).

2.3 Data reduction

The reduction of the optical photometry was performed using standard IRAF[2] tasks. The first reduction steps included bias, overscan and flat-field corrections, and the trimming of the images using the IRAF package CCDRED.

The pre-reduction of the NIR images was slightly more laborious, as it required a few additional steps. Due to the high luminosity of the night sky in the NIR, we needed to remove the sky contribution from the target images, by creating 'clean' sky images. This was done by

[2] IRAF is distributed by the National Optical Astronomy Observatories, which are operated by the Association of Universities for Research in Astronomy, Inc., under cooperative agreement with the National Science Foundation.

Table 2. U, B, V, R, I magnitudes of the sequence stars in the field of SN 2005cf. The errors reported in brackets are the rms of the available measurements, obtained during photometric nights only.

Star	U	B	V	R	I
1	14.886 (0.018)	14.710 (0.008)	13.986 (0.007)	13.561 (0.007)	13.155 (0.006)
2	18.243 (0.021)	18.125 (0.008)	17.308 (0.007)	16.867 (0.008)	16.453 (0.006)
3	19.217 (0.015)	18.292 (0.009)	17.262 (0.007)	16.682 (0.008)	16.178 (0.006)
4	18.080 (0.020)	17.548 (0.011)	16.661 (0.007)	16.164 (0.008)	15.705 (0.006)
5	19.290 (0.013)	18.131 (0.009)	16.705 (0.005)	15.800 (0.005)	14.930 (0.007)
6		17.176 (0.008)	17.005 (0.008)	16.940 (0.012)	16.829 (0.007)
7	17.314 (0.020)	17.172 (0.010)	16.350 (0.006)	15.895 (0.008)	15.436 (0.006)
8	19.128 (0.022)	18.207 (0.009)	17.152 (0.008)	16.552 (0.006)	16.035 (0.007)
9	20.984 (0.059)	19.776 (0.010)	18.490 (0.012)	17.605 (0.007)	16.795 (0.006)
10	15.865 (0.009)	15.827 (0.011)	15.169 (0.007)	14.777 (0.005)	14.423 (0.006)
11	16.917 (0.010)	16.929 (0.006)	16.264 (0.007)	15.883 (0.006)	15.523 (0.010)
12	17.475 (0.011)	17.503 (0.008)	16.837 (0.007)	16.458 (0.007)	16.109 (0.005)
13	17.668 (0.016)	16.688 (0.008)	15.662 (0.007)	15.066 (0.006)	14.573 (0.009)
14	19.939 (0.018)	18.879 (0.009)	17.271 (0.010)	16.300 (0.008)	15.167 (0.010)
15	17.627 (0.011)	17.398 (0.009)	16.543 (0.009)	16.058 (0.008)	15.602 (0.005)
16	16.446 (0.011)	16.401 (0.010)	15.700 (0.007)	15.288 (0.006)	14.909 (0.008)
17	18.181 (0.016)	18.456 (0.009)	17.863 (0.007)	17.487 (0.009)	17.153 (0.007)
18	15.228 (0.019)	14.717 (0.008)	13.833 (0.006)	13.298 (0.006)	12.786 (0.008)
19	17.808 (0.013)	17.952 (0.008)	17.397 (0.009)	17.031 (0.007)	16.695 (0.007)
20	16.556 (0.022)	15.813 (0.006)	14.801 (0.005)	14.201 (0.005)	13.676 (0.007)

median-combining a number of dithered science frames. The resulting sky template image was then subtracted from the target images. Most of our data were obtained with several short-exposure dithered frames, which had to be spatially registered and then combined in order to improve the S/N.

The NICS images required particular treatment, as they needed also to be corrected for the cross talking effect (i.e. a signal which was detected in one quadrant produced negative ghost images in the other three quadrants) and for the distortion of the NICS optics. These corrections were performed using a pipeline, SNAP,[3] available at TNG for the reduction of images obtained using NICS.

Instrumental magnitudes of SN 2005cf were determined with the point spread function (PSF) fitting technique, performed using the SNOOPY[4] package. Since SN 2005cf is a very bright and isolated object, the subtraction of the host galaxy template is not required, and the PSF fitting technique provides excellent results.

In order to transform instrumental magnitudes into the standard photometric system, first-order colour corrections were applied, using colour terms derived from observations of several photometric standard fields (Landolt 1992). The photometric zero-points were finally determined for all nights by comparing magnitudes of a local sequence of stars in the vicinity of the host galaxy (cf. Fig. 1) to the average estimates obtained during some photometric nights. The average magnitudes for the sequence stars in the field of SN 2005cf are reported in Table 2.

The data from Anupama et al. (in preparation) have been checked comparing the stars in common to both local sequences. In order to calibrate their SN magnitudes on to our sequence, we applied additive zero-point shifts (smaller than 0.05 mag), slightly corrected for the colour terms of the instrumental configuration of HCT.

In analogy to optical observations, NIR photometry was computed using different standard fields of the Arnica catalogue (Hunt et al. 1998) and finally calibrated using a number of local standards in the field of SN 2005cf (Fig. 2). The J, H, K' magnitudes of the IR local standards are reported in Table 3.

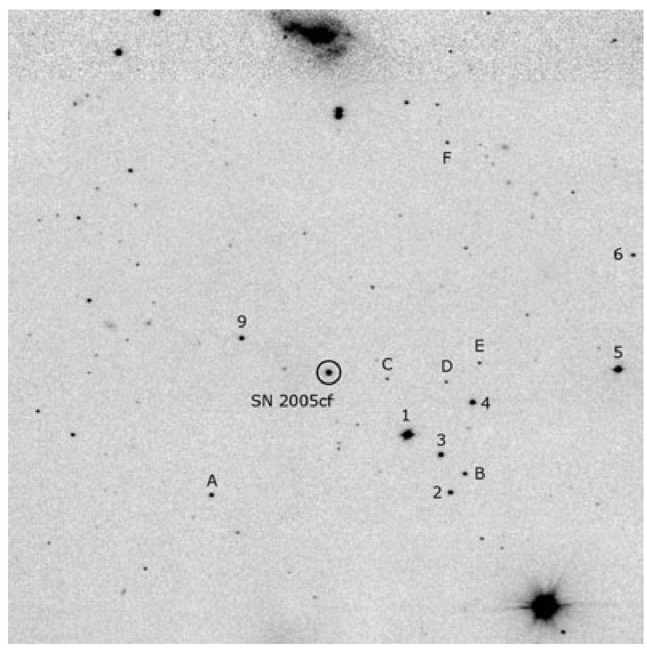

Figure 2. SN 2005cf in MCG-01-39-003: H-band image obtained on 2005 July 14 with the Telescopio Nazionale Galileo (TNG) of La Palma (Canary Islands) equipped with NICS. The field of view is 4.2×4.2 arcmin^2. The NIR sequence stars reported in Table 3 are labelled. North is up, east is to the left-hand side.

3 LIGHT CURVES OF SN 2005CF

3.1 *S*-correction to the optical light curves

The optical photometry of SN 2005cf, as derived from comparison with the Landolt's standard fields and our local sequence stars

[3] http://www.arcetri.astro.it/∼filippo/snap/
[4] SNOOPY is a package originally designed by F. Patat, implemented in IRAF by E. Cappellaro and based on DAOPHOT.

Table 3. J, H, K' magnitudes of the sequence stars in the field of SN 2005cf, with assigned errors.

Star	J	H	K'
1	12.54 (0.01)	12.15 (0.02)	12.21 (0.01)
2	15.91 (0.01)	15.46 (0.02)	15.53 (0.03)
3	15.49 (0.01)	14.97 (0.01)	14.99 (0.02)
4	15.10 (0.02)	14.61 (0.02)	14.60 (0.01)
5	13.84 (0.08)	13.22 (0.01)	13.25 (0.03)
6	16.74 (0.01)	16.50 (0.01)	
9	15.80 (0.01)	15.07 (0.03)	15.01 (0.02)
A	16.56 (0.03)	15.88 (0.04)	15.85 (0.04)
B	16.85 (0.03)	16.27 (0.03)	16.12 (0.01)
C	17.70 (0.03)	17.31 (0.02)	17.34 (0.01)
D	17.77 (0.03)	17.36 (0.04)	17.40 (0.01)
E	17.62 (0.01)	17.26 (0.02)	17.27 (0.07)
F	17.39 (0.01)	17.26 (0.07)	

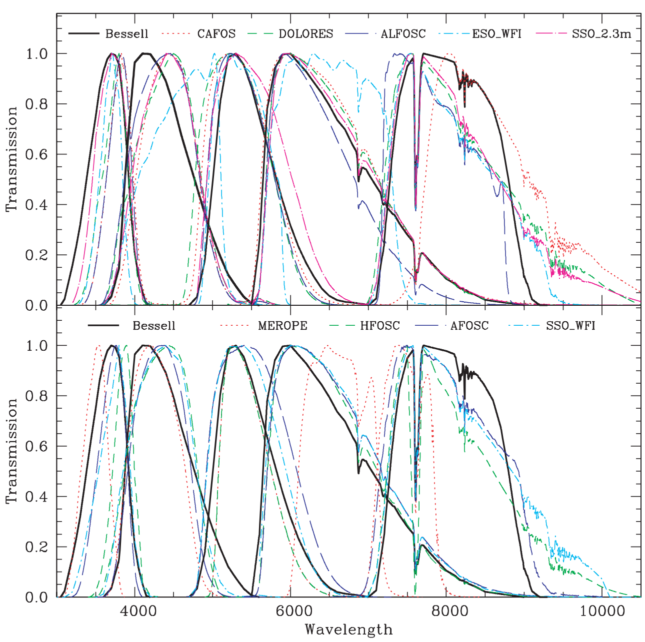

Figure 3. Comparison between the different instrumental U, B, V, R and I transmission curves, normalized to the peak transmission, and the standard Johnson–Cousins functions. The instrumental transmission curves were reconstructed taking into account the filter transmission, the CCD quantum efficiency, the reflectivity of the mirrors, the atmospheric transmission and, when available, the lenses throughput.

only (see below), shows a disturbing scatter in the magnitudes obtained using different instrumental configurations. This was due to the combination of the difference between the instrumental photometric system (see also Fig. 3) and the non-thermal SN spectrum. In order to remove these systematic errors we used a technique, presented in Stritzinger et al. (2002), called *S*-correction. To compute the corrections, one first needs to determine the instrumental passband $S(\lambda)$, defined as

$$S(\lambda) = F(\lambda) QE(\lambda) A(\lambda) M(\lambda) L(\lambda), \quad (1)$$

where $F(\lambda)$ is the filter transmission function, $QE(\lambda)$ is the detector quantum efficiency, $A(\lambda)$ is the continuum atmospheric transmission profile, $M(\lambda)$ is the mirror reflectivity function and $L(\lambda)$ is the lens throughput. Information on instruments, detectors and filters used during the follow-up of SN 2005cf is given in Section 2.2. In order to derive the atmospheric transmission profile of Calar Alto and La Palma, we made use of the information reported in Hopp & Fernàndez (2002) and King (1985), respectively, while for the La Silla site we used the CTIO transmission curve available in IRAF. For Asiago–Ekar, the Siding Spring Observatory and the Indian Astronomical Observatory we obtained $A(\lambda)$ by adapting the standard atmospheric model proposed by Walker (1987) in order to match the average broad-band absorption coefficients of these sites. Finally, $M(\lambda)$ was obtained using a standard aluminium reflectivity curve multiplied by the number of reflections in a given instrumental configuration, while $L(\lambda)$ was estimated for DOLORES and WFI only. For all the other instrumental configurations, we assumed that $L(\lambda)$ was constant across the whole spectral range. This approximation, together with a rapid variability both in the CCD quantum efficiency and in the atmosphere's transmission curve at the blue wavelengths, are probably the reasons why the U reconstructed passbands do not match the observed ones (see Table 4).

In order to check the match between the modelled passbands and the real ones, and to calculate the instrumental zero-points for all configurations, we followed the same approach as Pignata et al. (2004), updating to the new set of spectrophotometric standard stars from Stritzinger et al. (2005), which span a range in colour larger than that provided by previous works (e.g. Hamuy et al. 1994). In Table 4 we report the comparison between the colour terms[5] computed via the synthetic photometry and those determined through the observation of a number of standard fields. For the latter, the estimates and their associated errors (see Table 4) were computed using a 3σ-clipped average. In a few cases, when the difference between the synthetic colour term and photometric colour term was larger than 3σ, the passbands were adjusted.

For each instrumental configuration, the *S*-correction measurements at different epochs were fitted by a third- or fourth-order polynomial, as in Pignata et al. (2004), and the rms deviations of the data points from the fitted law provided an estimate of the errors due to the correction itself. The correction applied to the photometry of SN 2005cf turned out to be effective because of the detailed characterization of the photometric properties of most of the instruments used by the ESC (Pignata et al. 2004) and the excellent spectral sequence available for this object (Garavini et al., in preparation). Note that, however, since most spectra of SN 2005cf had not adequate coverage in the region below 3500 Å, we had to resort to spectra of SN 1994D in order to estimate the *S*-correction for the U band.

The original (i.e. non-*S*-corrected) optical photometry for SN 2005cf is reported in Table 5 (Columns 3–7). The corrections to be applied to the original magnitudes are also reported in Table 5 (Columns 8–12). The differences are in general quite small, especially in the B, V, R bands, and they are significant only for some specific instrumental configurations (sometimes of 0.1–0.2 mag, see e.g. the I filters of the Mercator Telescope + Merope, the 2.2-m Calar Alto Telescope + CAFOS and the Himalayan *Chandra* Telescope + HFOSC or the B filter mounted at the 2.2-m ESO/MPI Telescope + WFI). On the contrary, the U-band correction is large for most instrumental configurations. As shown in Fig. 3 (see also Stanishev et al. 2006), this is because the sensitivity curves of the U filters available at the various telescopes are significantly different (being

[5] The colour term is the coefficient B of the equation $m_{\lambda 1} = m^{ST}_{\lambda 1} + A + B(m_{\lambda 2} - m_{\lambda 1})$ which is used to calibrate instrumental magnitude $m^{ST}_{\lambda 1}$ to the standard system $m_{\lambda 1}$.

Table 4. Comparison between synthetic and photometric colour terms. The colour terms for HFOSC are provided by the observatory without associated errors. For SSO 40-in. Telescope + WFI, we have only two colour term measurements, therefore the statistic is too poor to compute reliable errors.

Instrument	$U(U-B)$		$B(B-V)$		$V(B-V)$		$R(V-R)$		$I(R-I)$	
	syn	ph	syn	ph	syn	ph	syn	ph	syn	ph
40 in. + WFI			−0.022	0.005	−0.002	0.033	0.054	0.054	0.042	−0.019
DOLORES	0.059[a]	0.105 ± 0.047	0.080	0.064 ± 0.018	−0.101	−0.120 ± 0.033	0.031	0.022 ± 0.037	0.025	0.023 ± 0.017
ALFOSC	0.093[a]	0.122 ± 0.010	0.023	0.044 ± 0.012	−0.048	−0.049 ± 0.021	−0.074	−0.098 ± 0.024	−0.086	−0.068 ± 0.033
2.3 m + imager	0.048	0.094 ± 0.033	0.081	0.014 ± 0.024	0.026	0.027 ± 0.009	0.035	0.040 ± 0.016	0.028	0.002 ± 0.016
Merope	−0.089	−0.105 ± 0.008	−0.168	−0.130 ± 0.014	−0.002	−0.001 ± 0.011	0.126	0.134 ± 0.022	−0.284	−0.332 ± 0.026
CAFOS	0.121[a]	0.167 ± 0.016	0.107	0.115 ± 0.005	−0.061	−0.048 ± 0.005	−0.008	−0.015 ± 0.017	0.219	0.256 ± 0.036
AFOSC			−0.068[a]	−0.030 ± 0.013	0.041	0.047 ± 0.010	0.066	0.052 ± 0.033	−0.031	−0.044 ± 0.036
2.2 m + WFI	−0.021	−0.070 ± 0.036	0.249	0.244 ± 0.024	−0.067	−0.067 ± 0.013	0.015	0.000 ± 0.022	−0.010	0.006 ± 0.022
HFOSC	0.155	0.188	−0.028	−0.049	0.045	0.047	0.038	0.065	0.018	0.017

[a]The passband's blue cut-off was modified.

Table 5. Original U, B, V, R, I magnitudes of SN 2005cf (Columns 3–7) and S-corrections (Columns 8–12) to be *added* to the original magnitudes to obtain the final, S-corrected optical magnitudes of SN 2005cf.

Date	JD (+240 0000)	Original magnitude U	B	V	R	I	S-correction ΔU	ΔB	ΔV	ΔR	ΔI	S
31/5	53521.90		15.493	15.243	15.142	15.191		−0.031	−0.005	−0.004	−0.014	1
31/5	53522.38	15.490	15.299	15.127	14.973	14.952	0.235	−0.027	−0.030	0.003	0.047	2
01/6	53522.97		15.044	14.902	14.785	14.819		−0.032	−0.004	−0.005	−0.014	1
01/6	53523.16	14.999	14.934	14.913	14.769	14.759	0.282	−0.010	−0.011	0.002	0.030	H
02/6	53524.13	14.613	14.609	14.658	14.466	14.472	0.234	−0.009	−0.009	0.001	0.029	H
02/6	53524.44	14.443	14.582	14.514	14.377	14.449	0.198	−0.021	−0.007	0.006	−0.011	3
03/6	53524.97		14.425	14.382	14.241	14.282		−0.033	−0.003	−0.005	−0.013	1
03/6	53525.25		14.348	14.373	14.224	14.214		−0.009	−0.006	0	0.028	H
04/6	53526.35		14.139	14.189	14.009	14.007		−0.008	−0.004	−0.002	0.028	H
06/6	53527.57	13.638	13.924	13.943	13.823	13.831	0.043	−0.026	−0.034	−0.001	0.035	2
06/6	53527.95		13.896	13.896	13.736	13.816		−0.034	−0.002	−0.006	−0.014	1
06/6	53528.14		13.848	13.944	13.792	13.822		−0.007	−0.001	−0.004	0.027	H
07/6	53529.24	13.533	13.730	13.822	13.680	13.758	0.063	−0.006	0.002	−0.005	0.027	H
08/6	53530.38	13.399	13.712	13.710	13.544	13.726	0.050	−0.018	−0.012	0.012	−0.029	3
08/6	53530.38	13.470	13.676	13.753	13.617	13.719	0.063	−0.006	0.003	−0.007	0.026	H
09/6	53531.12		13.614	13.695	13.597	13.688		−0.005	0.004	−0.007	0.025	H
09/6	53531.48		13.659	13.629		13.737		−0.017	−0.013		−0.034	3
10/6	53531.52				13.501					0.013		3
10/6	53532.19		13.601	13.628	13.553	13.689		−0.004	0.004	−0.008	0.025	H
11/6	53533.13	13.410	13.539	13.618	13.541	13.696	0.078	−0.004	0.004	−0.009	0.024	H
12/6	53533.50	13.320	13.602	13.592	13.432	13.706	0.067	−0.015	−0.012	0.015	−0.042	3
12/6	53533.99	13.423	13.568	13.525	13.462	13.748	0.044	−0.029	−0.002	−0.007	−0.022	4
14/6	53536.47	13.570	13.602	13.501	13.486	13.990	0.001	−0.008	0.022	−0.041	−0.184	5
16/6	53538.19	13.645		13.606	13.558	13.831	0.112		−0.005	−0.007	0.031	H
16/6	53538.36	13.540	13.725	13.581	13.562	13.688	0.155	−0.036	−0.023	0.004	0.158	6
17/6	53539.21		13.723	13.641	13.583	13.864		−0.003	−0.008	−0.007	0.033	H
17/6	53539.37	13.628	13.798	13.616	13.567	13.700	0.166	−0.034	−0.022	0.004	0.164	6
18/6	53540.13		13.770	13.664	13.625	13.931		−0.003	−0.010	−0.006	0.036	H
18/6	53540.41	13.714	13.887	13.656	13.607	13.780	0.178	−0.032	−0.021	0.004	0.172	6
19/6	53541.37	13.790	13.929	13.713	13.653	13.828	0.189	−0.030	−0.020	0.004	0.180	6
20/6	53542.26	13.909	13.925	13.743	13.742	14.030	0.158	−0.004	−0.016	−0.003	0.041	H
21/6	53542.53	13.831	14.144	13.724	13.695	13.885	0.201	−0.029	−0.019	0.004	0.189	6
21/6	53543.14	14.013	14.050	13.781	13.814	14.083	0.165	−0.005	−0.018	−0.001	0.043	H
22/6	53543.51	14.450	14.065	13.694	13.764	14.432	−0.146	−0.012	0.033	−0.028	−0.254	5
23/6	53545.13	14.246	14.197	13.915	13.906	14.212	0.177	−0.006	−0.023	0.001	0.047	H
24/6	53546.30	14.296	14.330	13.974	14.031	14.267	0.179	−0.007	−0.025	0.002	0.049	H
24/6	53546.36	14.294	14.386	13.921	13.974	14.067	0.219	−0.028	−0.012	0.004	0.198	6
24/6	53546.43	14.420	14.368	13.937	13.950	14.394	0.163	−0.007	0.003	0.022	−0.087	3

often shifted to redder wavelengths) compared to the standard U Bessell passband.

We remark that S-correction in the U band is affected by a non-negligible uncertainty due to the low quantum efficiency of the CCDs and errors in the flux calibration of the SN spectra below ∼3500 Å.

The comparison between the U and the I-band light curves of SN 2005cf (Fig. 4, top and bottom, respectively) before and after

Table 5 – *continued*

Date	JD	Original magnitude					*S*-correction					S
	(+240 0000)	*U*	*B*	*V*	*R*	*I*	Δ*U*	Δ*B*	Δ*V*	Δ*R*	Δ*I*	
25/6	53546.50	14.859	14.376	13.879	13.986		−0.177	−0.014	0.036	−0.018		5
25/6	53547.45	14.409	14.523	13.996	14.060	14.111	0.219	−0.028	−0.010	0.004	−0.199	6
26/6	53548.40	14.512	14.626	13.990	14.105	14.126	0.219	−0.029	−0.009	0.005	0.197	6
28/6	53550.37	14.858	14.877	14.164	14.170	14.143	0.219	−0.033	−0.005	0.005	0.189	6
29/6	53551.48	15.593	14.919	14.169	14.143	14.573	−0.195	−0.019	0.036	−0.005	−0.170	5
01/7	53553.37	15.275	15.224	14.333	14.240	14.142	0.218	−0.040	0.001	0.006	0.164	6
02/7	53554.37	15.383	15.307	14.356	14.219	14.124	0.218	−0.042	0.003	0.007	0.159	6
03/7	53555.47	16.099	15.364	14.385	14.196	14.308	−0.209	−0.024	0.034	0.005	−0.101	5
06/7	53558.48	16.331	15.640	14.558	14.287	14.250	−0.220	−0.024	0.032	0.004	−0.053	5
07/7	53559.19	15.957	15.751	14.680	14.331	14.130	0.183	−0.025	−0.020	−0.011	0.062	H
07/7	53559.49	16.059	15.812	14.593	14.280	14.237	0.166	−0.015	0.021	0.007	−0.049	3
10/7	53562.48	16.645	15.972	14.763	14.402	14.151	−0.234	−0.020	0.031	−0.001	−0.004	5
11/7	53563.24	16.220	16.079	14.889	14.495	14.095	0.184	−0.026	−0.015	−0.018	0.062	H
11/7	53563.37	16.253	16.135	14.850	14.459	14.143	0.216	−0.067	0.011	0.010	0.113	6
12/7	53564.37	16.324	16.226	14.923	14.515	14.180	0.215	−0.068	0.011	0.010	0.114	6
13/7	53564.50	16.837	16.113	14.902	14.492	14.260	−0.241	−0.018	0.031	−0.004	0.012	5
14/7	53566.41		16.327	15.066	14.633	14.291		−0.010	−0.024	−0.019	0.035	7
18/7	53569.57	16.831	16.592	15.179	14.863	14.444	−0.065	−0.096	0.056	−0.027	0.044	8
20/7	53571.60	16.945	16.684	15.298	14.977	14.599	−0.066	−0.097	0.054	−0.029	0.044	8
20/7	53572.21		16.616	15.430	15.071	14.650		−0.023	−0.009	−0.023	0.072	H
22/7	53573.55	16.965	16.753	15.384	15.097	14.727	−0.066	−0.097	0.051	−0.032	0.045	8
23/7	53575.20	16.753	16.660	15.546	15.204	14.810	0.190	−0.020	−0.008	−0.023	0.076	H
24/7	53575.51	17.002	16.799	15.471	15.193	14.827	−0.066	−0.096	0.048	−0.034	0.046	8
27/7	53578.55	17.086	16.891	15.574	15.327	14.977	−0.065	−0.094	0.043	−0.038	0.048	8
30/7	53581.61	17.152	16.914	15.659	15.417	15.129	−0.064	−0.091	0.039	−0.042	0.051	8
31/7	53583.41	16.996	16.862	15.755	15.443	15.299	0.182	−0.014	0.016	0.011	−0.018	3
01/8	53584.20		16.833	15.823	15.543	15.275		−0.022	−0.010	−0.020	0.084	H
04/8	53587.14	16.997	16.897	15.881	15.660	15.378	0.201	−0.025	−0.012	−0.018	0.086	H
05/8	53587.56	17.258	17.005	15.873	15.619	15.392	−0.062	−0.092	0.033	−0.044	0.056	8
08/8	53590.56	17.300	17.076	15.929	15.733	15.522	−0.061	−0.092	0.031	−0.044	0.059	8
08/8	53591.13		16.970	16.006	15.763	15.575		−0.027	−0.015	−0.016	0.089	H
13/8	53595.50	17.369	17.094	16.075	15.868	15.681	−0.061	−0.089	0.028	−0.043	0.062	8
14/8	53597.10				15.978					−0.012		H
15/8	53598.38	17.275	17.096	16.172	15.943	15.886	0.187	−0.008	0.014	0.018	0.009	3
17/8	53600.18					15.992					0.096	H
21/8	53604.15		17.192	16.368	16.173	16.109		−0.022	−0.020	−0.008	0.099	H
28/8	53611.38	17.410	17.294	16.475	16.372	16.518	0.235	−0.003	−0.008	−0.001	0.091	6
30/8	53613.37	17.576	17.293	16.519	16.385	16.464	0.183	0.023	0.008	0.020	0.036	3
01/9	53615.14			16.618	16.525	16.561			−0.020	0.001	0.109	H
03/9	53617.10		17.341	16.674	16.552	16.596		0	−0.020	0.003	0.112	H
07/9	53621.11	17.741	17.412	16.798	16.695	16.754	0.183	0.009	−0.020	0.007	0.116	H

Notes: 1 = 40-in. SSO Telescope + WFI; 2 = 3.5-m Telescopio Nazionale Galileo + DOLORES; 3 = 2.5-m Nordic Optical Telescope + ALFOSC; 4 = 2.3-m SSO Telescope + imager; 5 = 1.2-m Mercator Telescope + MEROPE; 6 = 2.2-m Calar Alto Telescope + CAFOS; 7 = 1.82-m Copernico Telescope + AFOSC; 8 = 2.2-m ESO/MPI Telescope + WFI; H = 2-m Himalayan *Chandra* Telescope + HFOSC.

the *S*-correction, displays the improvement in the quality of the photometry. The final optical light curves are shown in Fig. 5, while the *S*-corrected magnitudes of SN 2005cf are reported in Table 6.

Hereafter, we will refer to Julian Date (JD) = 245 3534.0 as the epoch of the *B*-band maximum light (see Section 4).

3.2 Near-IR light curves

Contrary to the optical photometry, no *S*-correction was applied to our NIR photometry, owing to the lack of adequate time coverage of the NIR spectroscopy. The NIR photometry available for SN 2005cf is shown in Table 7. In Fig. 6, the absolute NIR light curves of SN 2005cf are compared with those of the well-studied SNe 2001el (Krisciunas et al. 2003) and 2002bo (Krisciunas et al. 2004). The absolute magnitudes were computed assuming the distance modulus and total reddening values of Table 8 (see Section 3.4).

SN 2002bo is significantly fainter than both SN 2005cf and 2001el. However, we remark that the behaviour of SN 2002bo in the NIR is rather peculiar and that SN 2005cf was observed in the K' band, while SN 2001el and SN 2002bo were calibrated by Krisciunas et al. (2003, 2004) in the standard Persson's system (Persson et al. 1998). The deep minimum in the *J*-band light curve of SN 2005cf resembles that observed in SN 2002bo, although the *J*-band luminosity is closer to that of SN 2001el. The plateau-like behaviour of the *H*-band light curve of SN 2005cf between phase about −10 and +30 is very similar to that observed in the light curve of SN 2001el. A strong similarity between SN 2005cf and SN 2001el is also seen in the *K*-band evolution. Their *K*-band light curves remain relatively flat from phase −10 and +30, while the maxima of SN 2002bo are somewhat more pronounced.

Recently, Kasen (2006) explained the variable strength of the NIR secondary maximum in SNe Ia in terms of different abundance

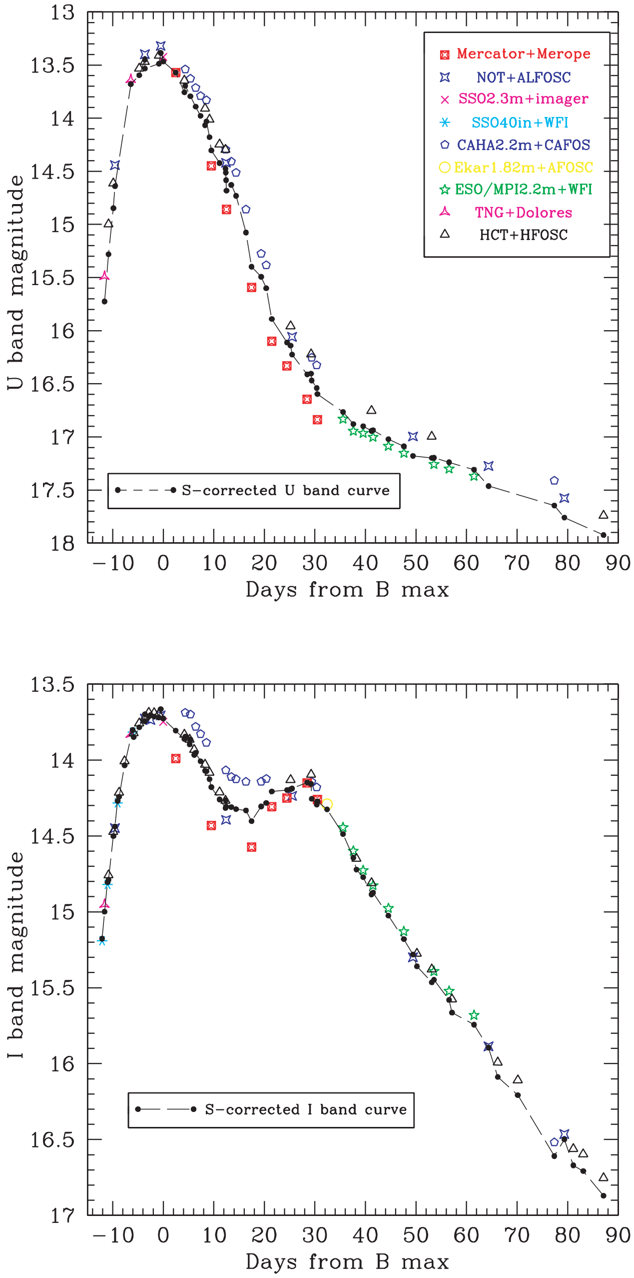

Figure 4. Top: comparison between the original *U*-band light curve of SN 2005cf and the *S*-corrected one. Bottom: the same, but for the *I* band. Original data points obtained using different instruments are plotted with different symbols. The large scatter is due to the diversity of the *U* and *I* filters available at the various telescopes. The final, *S*-corrected *U*- and *I*-band photometry is represented by filled circles, connected with a dashed line.

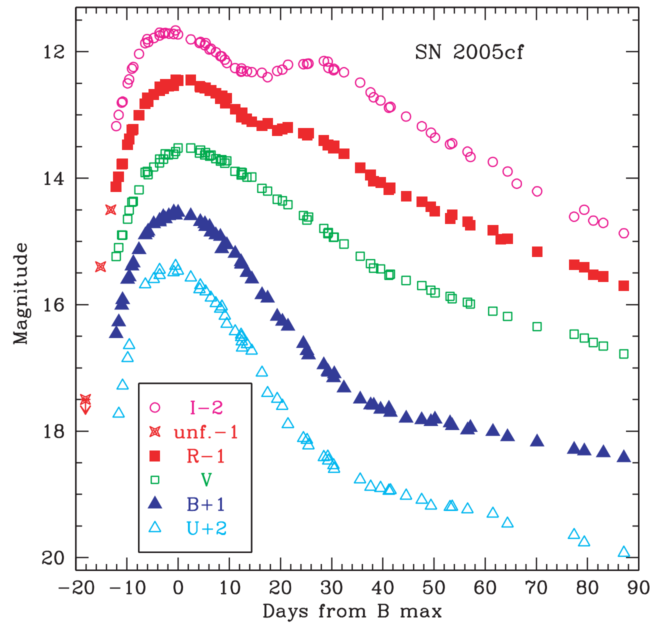

Figure 5. *U*, *B*, *V*, *R*, *I* light curves of SN 2005cf, including the unfiltered measurements from IAU Circ. 8534 (asterisk). The phase is measured in days from the *B*-band maximum.

stratification, metallicities of the progenitor star and amounts iron-group elements synthesized in the explosion. In particular, Type Ia SNe ejecting more radioactive ^{56}Ni are expected to show, together with a brighter light curve, more pronounced NIR secondary maxima.

3.3 Reddening and distance

SN 2005cf exploded very far from the nucleus of MCG-01-39-003, in a region with low background contamination. Deep late-time VLT imaging (F. Patat, private communication) shows that the SN exploded at the edge of a long tidal bridge connecting MCG-01-39-003 with the interacting companion (see also Vorontsov-Velyaminov & Arhipova 1963), suggesting relatively small host galaxy interstellar extinction. This finding is supported by non-detection of narrow interstellar lines in the SN spectra. As Section 3.4 will show, a small value for the interstellar extinction is also supported by the normal colour curves of SN 2005cf. Therefore, in this paper we will adopt as total extinction the Galactic estimate at the coordinates of the SN, that is, $E(B-V) = 0.097 \pm 0.010$, reported by Schlegel, Finkbeiner & Davis (1998).

Despite the relatively short distance, the galaxy system hosting SN 2005cf is poorly studied. As a consequence, large uncertainty exists in the distance estimate. For MCG-01-39-003 and NGC 5917 LEDA provides the recession velocities corrected for the effects of the Local Group infall on to the Virgo Cluster (208 km s^{-1}, Terry, Paturel & Ekholm 2002): $v_{\rm Vir} = 1977$ and 1944 km s^{-1} are reported for the two galaxies, respectively. However, we should take into account a non-negligible gravitational effect of the Virgo Cluster at the distance of the two galaxies. Taking into account the observed positions of the two galaxies relative to the Virgo centre, a crude estimate of the virgocentric component subtracts to the observed recession velocities about 3–400 km s^{-1}.

Kraan-Korteweg (1986) computed distance estimates of a large sample of nearby galaxies based on a virgocentric non-linear flow model (see e.g. Silk 1977). While MCG-01-39-003 and NGC 5917 are not listed in the catalogue, with a good approximation we can assume the same infalling correction computed for another galaxy, NGC 5812, which projects very close to the SN 2005cf parent galaxy and has similar recession velocity ($v_{\rm Vir} = 1965$ km s^{-1}, LEDA, cf. Table 1). In the Kraan-Korteweg's catalogue, the distances are expressed in units of the Virgo Cluster distance ($d_{\rm Vir}$). For NGC 5812 two alternative distances are derived from different assumptions on the virgocentric infalling velocity of the Local Group: 1.91$d_{\rm Vir}$ for a more commonly accepted 220 km s^{-1} – model (Tammann

Table 6. Final, *S*-corrected *U*, *B*, *V*, *R*, *I* magnitudes of SN 2005cf. The uncertainties reported in brackets take into account both measurement and photometric calibration errors. Unfiltered measurements from IAU Circ. 8534 are also reported.

Date	JD (+240 0000)	*U*	*B*	*V*	*R*	*I*	S
25/5	53515.87				⩾18.5		0
28/5	53518.86				16.4		0
30/5	53520.85				15.5		0
31/5	53521.90		15.462 (0.010)	15.238 (0.008)	15.138 (0.009)	15.177 (0.011)	1
31/5	53522.38	15.725 (0.043)	15.272 (0.015)	15.097 (0.010)	14.976 (0.011)	14.999 (0.024)	2
01/6	53522.97		15.012 (0.009)	14.898 (0.008)	14.780 (0.008)	14.805 (0.009)	1
01/6	53523.16	15.281 (0.055)	14.924 (0.017)	14.902 (0.020)	14.771 (0.013)	14.789 (0.024)	H
02/6	53524.13	14.847 (0.053)	14.600 (0.024)	14.649 (0.024)	14.467 (0.016)	14.501 (0.022)	H
02/6	53524.44	14.641 (0.044)	14.561 (0.011)	14.507 (0.009)	14.383 (0.009)	14.438 (0.010)	3
03/6	53524.97		14.392 (0.010)	14.379 (0.007)	14.236 (0.008)	14.269 (0.009)	1
03/6	53525.25		14.339 (0.041)	14.367 (0.015)	14.224 (0.011)	14.242 (0.020)	H
04/6	53526.35		14.131 (0.041)	14.185 (0.034)	14.007 (0.012)	14.035 (0.023)	H
06/6	53527.57	13.681 (0.045)	13.899 (0.015)	13.909 (0.013)	13.822 (0.010)	13.866 (0.023)	2
06/6	53527.95		13.862 (0.012)	13.894 (0.010)	13.730 (0.011)	13.802 (0.013)	1
06/6	53528.14		13.841 (0.012)	13.943 (0.021)	13.788 (0.017)	13.849 (0.018)	H
07/6	53529.24	13.596 (0.048)	13.724 (0.011)	13.824 (0.020)	13.675 (0.011)	13.785 (0.019)	H
08/6	53530.38	13.449 (0.044)	13.694 (0.011)	13.698 (0.008)	13.556 (0.009)	13.697 (0.009)	3
08/6	53530.38	13.533 (0.062)	13.670 (0.018)	13.756 (0.021)	13.610 (0.014)	13.745 (0.030)	H
09/6	53531.12		13.609 (0.029)	13.699 (0.024)	13.590 (0.014)	13.713 (0.020)	H
09/6	53531.48		13.642 (0.011)	13.617 (0.011)		13.703 (0.010)	3
10/6	53531.52				13.514 (0.013)		3
10/6	53532.19		13.597 (0.039)	13.632 (0.020)	13.545 (0.013)	13.714 (0.027)	H
11/6	53533.13	13.487 (0.047)	13.535 (0.029)	13.622 (0.028)	13.533 (0.019)	13.720 (0.018)	H
12/6	53533.50	13.386 (0.044)	13.587 (0.010)	13.580 (0.009)	13.447 (0.011)	13.664 (0.010)	3
12/6	53533.99	13.467 (0.029)	13.539 (0.010)	13.523 (0.011)	13.455 (0.012)	13.727 (0.047)	4
14/6	53536.47	13.571 (0.065)	13.594 (0.010)	13.523 (0.008)	13.445 (0.015)	13.806 (0.035)	5
16/6	53538.19	13.757 (0.056)		13.601 (0.022)	13.551 (0.016)	13.862 (0.019)	H
16/6	53538.36	13.695 (0.049)	13.689 (0.013)	13.558 (0.013)	13.566 (0.015)	13.846 (0.030)	6
17/6	53539.21		13.720 (0.022)	13.633 (0.027)	13.577 (0.016)	13.897 (0.016)	H
17/6	53539.37	13.794 (0.049)	13.764 (0.013)	13.594 (0.008)	13.571 (0.010)	13.864 (0.028)	6
18/6	53540.13		13.767 (0.019)	13.654 (0.026)	13.620 (0.015)	13.966 (0.023)	H
18/6	53540.41	13.892 (0.049)	13.855 (0.013)	13.635 (0.011)	13.611 (0.012)	13.952 (0.031)	6
19/6	53541.37	13.979 (0.049)	13.899 (0.016)	13.693 (0.015)	13.657 (0.012)	14.008 (0.032)	6
20/6	53542.26	14.067 (0.057)	13.921 (0.024)	13.727 (0.015)	13.739 (0.032)	14.071 (0.024)	H
21/6	53542.53	14.032 (0.050)	14.115 (0.018)	13.705 (0.015)	13.700 (0.013)	14.074 (0.030)	6
21/6	53543.14	14.178 (0.060)	14.045 (0.022)	13.763 (0.025)	13.813 (0.014)	14.126 (0.018)	H
22/6	53543.51	14.304 (0.065)	14.053 (0.009)	13.727 (0.009)	13.736 (0.015)	14.179 (0.022)	5
23/6	53545.13	14.423 (0.053)	14.191 (0.025)	13.892 (0.024)	13.907 (0.016)	14.259 (0.033)	H

& Sandage 1985) or $1.84d_{\rm Vir}$ for a 440 km s^{-1} – model (Kraan-Korteweg 1986). Since a value for the local infalling velocity towards Virgo of 220 km s^{-1} is close to that currently adopted by LEDA (208 km s^{-1}), hereafter we will adopt the first infalling velocity model.

To derive the distance modulus of SN 2005cf we need to adopt a distance for Virgo. For the latter, the values reported in the literature show some scatter. For instance, the mean Tully–Fisher distance of Virgo obtained by Fouqué et al. (2001) from 51 spiral galaxies members of the cluster is $d = 18.0 \pm 1.2$ Mpc. This gives a distance of NGC 5812 of 34.4 Mpc ($\mu = 32.68$).

Alternatively, computing the Cepheid distances of six galaxies of the Virgo Cluster, Fouqué et al. (2001) found a somewhat smaller distance of Virgo: $d = 15.4 \pm 0.5$ Mpc. The resulting distance of NGC 5812 is 29.4 Mpc ($\mu = 32.34$). Averaging the distance moduli of NGC 5812 obtained from the two different estimates of the Virgo distance, we obtain $\mu = 32.51$. We can reasonably adopt this distance modulus also for MCG-01-39-003 and NGC 5917. A conservative estimate of the error is obtained from the dispersion of the galaxy peculiar motions, that is, ∼350 km s^{-1} (Somerville, Davis & Primack 1997), which gives a maximum error in the distance modulus of $\Delta\mu = 0.33$. Hereafter, we will adopt $\mu = 32.51 \pm 0.33$ as our best distance modulus estimate for the galaxy hosting SN 2005cf.

3.4 Colour curves, absolute luminosity and bolometric light curve

In what follows, we compare colour evolution, absolute light curves and pseudo-bolometric luminosity of SN 2005cf with those of other Type Ia SNe with similar light-curve shape. The range of $\Delta m_{15}(B) \sim 1.0$–1.2 (around the average value for normal SNe Ia) is well populated. As comparison objects we have selected SNe 1992al (Hamuy et al. 1996), 2001el (Krisciunas et al. 2003), 2002bo (Benetti et al. 2004; Krisciunas et al. 2004) and 2002dj (Pignata et al., in preparation). Basic information about the distance moduli and reddening values adopted for this sample is reported in Table 8. In particular, as already seen in Section 3.3, $\mu = 32.51$ and $E(B - V) = 0.097$ (Schlegel et al. 1998) were adopted for SN 2005cf.

Table 6 – *continued*

Date	JD (+240 0000)	*U*	*B*	*V*	*R*	*I*	S
24/6	53546.30	14.475 (0.052)	14.323 (0.017)	13.949 (0.022)	14.033 (0.026)	14.316 (0.030)	H
24/6	53546.36	14.513 (0.049)	14.358 (0.016)	13.909 (0.011)	13.978 (0.015)	14.265 (0.030)	6
24/6	53546.43	14.583 (0.044)	14.361 (0.011)	13.940 (0.012)	13.972 (0.010)	14.307 (0.017)	3
25/6	53546.50	14.682 (0.065)	14.362 (0.009)	13.915 (0.008)	13.968 (0.015)		5
25/6	53547.45	14.628 (0.049)	14.495 (0.012)	13.986 (0.009)	14.064 (0.010)	14.310 (0.029)	6
26/6	53548.40	14.731 (0.050)	14.597 (0.014)	13.981 (0.009)	14.110 (0.012)	14.323 (0.031)	6
28/6	53550.37	15.076 (0.049)	14.844 (0.013)	14.159 (0.009)	14.175 (0.008)	14.332 (0.028)	6
29/6	53551.48	15.398 (0.065)	14.900 (0.009)	14.205 (0.007)	14.139 (0.015)	14.403 (0.022)	5
01/7	53553.37	15.493 (0.050)	15.184 (0.013)	14.334 (0.013)	14.246 (0.015)	14.306 (0.032)	6
02/7	53554.37	15.601 (0.050)	15.265 (0.014)	14.359 (0.013)	14.226 (0.016)	14.283 (0.032)	6
03/7	53555.47	15.890 (0.065)	15.340 (0.009)	14.419 (0.008)	14.201 (0.015)	14.207 (0.021)	5
06/7	53558.48	16.111 (0.066)	15.616 (0.009)	14.590 (0.008)	14.291 (0.015)	14.197 (0.022)	5
07/7	53559.19	16.140 (0.050)	15.726 (0.018)	14.660 (0.023)	14.320 (0.011)	14.192 (0.015)	H
07/7	53559.49	16.225 (0.044)	15.797 (0.010)	14.614 (0.008)	14.287 (0.010)	14.188 (0.009)	3
10/7	53562.48	16.411 (0.065)	15.952 (0.010)	14.794 (0.008)	14.401 (0.015)	14.147 (0.022)	5
11/7	53563.24	16.404 (0.059)	16.053 (0.013)	14.874 (0.026)	14.477 (0.018)	14.157 (0.029)	H
11/7	53563.37	16.469 (0.051)	16.069 (0.013)	14.861 (0.010)	14.469 (0.011)	14.255 (0.031)	6
12/7	53564.37	16.539 (0.049)	16.158 (0.013)	14.934 (0.010)	14.525 (0.009)	14.294 (0.029)	6
13/7	53564.50	16.596 (0.066)	16.095 (0.010)	14.933 (0.008)	14.488 (0.015)	14.272 (0.021)	5
14/7	53566.41		16.317 (0.015)	15.042 (0.017)	14.614 (0.021)	14.325 (0.026)	7
18/7	53569.57	16.766 (0.032)	16.496 (0.012)	15.235 (0.009)	14.836 (0.009)	14.488 (0.018)	8
20/7	53571.60	16.879 (0.030)	16.587 (0.011)	15.351 (0.009)	14.948 (0.009)	14.643 (0.018)	8
20/7	53572.21		16.593 (0.022)	15.421 (0.031)	15.048 (0.019)	14.721 (0.025)	H
22/7	53573.55	16.899 (0.030)	16.656 (0.011)	15.435 (0.009)	15.065 (0.008)	14.772 (0.017)	8
23/7	53575.20	16.943 (0.063)	16.640 (0.021)	15.538 (0.028)	15.181 (0.021)	14.885 (0.023)	H
24/7	53575.51	16.937 (0.029)	16.703 (0.011)	15.519 (0.009)	15.159 (0.009)	14.873 (0.018)	8
27/7	53578.55	17.021 (0.030)	16.797 (0.011)	15.617 (0.009)	15.289 (0.009)	15.025 (0.017)	8
30/7	53581.61	17.088 (0.030)	16.823 (0.012)	15.698 (0.009)	15.376 (0.009)	15.180 (0.018)	8
31/7	53583.41	17.178 (0.044)	16.849 (0.010)	15.771 (0.008)	15.454 (0.009)	15.281 (0.009)	3
01/8	53584.20		16.811 (0.027)	15.813 (0.028)	15.523 (0.011)	15.359 (0.035)	H
04/8	53587.14	17.198 (0.052)	16.872 (0.020)	15.869 (0.020)	15.642 (0.027)	15.464 (0.018)	H
05/8	53587.56	17.196 (0.030)	16.913 (0.011)	15.906 (0.009)	15.575 (0.009)	15.448 (0.018)	8
08/8	53590.56	17.239 (0.029)	16.984 (0.011)	15.960 (0.009)	15.689 (0.009)	15.580 (0.018)	8
08/8	53591.13		16.943 (0.013)	15.991 (0.022)	15.747 (0.013)	15.664 (0.026)	H
13/8	53595.50	17.308 (0.109)	17.005 (0.022)	16.103 (0.040)	15.825 (0.020)	15.743 (0.027)	8
14/8	53597.10				15.966 (0.018)		H
15/8	53598.38	17.462 (0.045)	17.088 (0.010)	16.186 (0.009)	15.961 (0.010)	15.895 (0.009)	3
17/8	53600.18					16.088 (0.021)	H
21/8	53604.15		17.171 (0.019)	16.348 (0.031)	16.165 (0.011)	16.208 (0.022)	H
28/8	53611.38	17.645 (0.051)	17.291 (0.013)	16.467 (0.011)	16.371 (0.009)	16.609 (0.030)	6
30/8	53613.37	17.759 (0.045)	17.316 (0.012)	16.527 (0.011)	16.405 (0.011)	16.500 (0.011)	3
01/9	53615.14			16.598 (0.019)	16.526 (0.014)	16.670 (0.030)	H
03/9	53617.10		17.341 (0.018)	16.654 (0.028)	16.555 (0.015)	16.707 (0.018)	H
07/9	53621.11	17.924 (0.053)	17.421 (0.021)	16.778 (0.025)	16.702 (0.015)	16.870 (0.025)	H

Notes: 0 = unfiltered magnitudes from IAU Circ. 8534; 1 = 40-in. SSO Telescope + WFI; 2 = 3.5-m Telescopio Nazionale Galileo + DOLORES; 3 = 2.5-m Nordic Optical Telescope + ALFOSC; 4 = 2.3-m SSO Telescope + imager; 5 = 1.2-m Mercator Telescope + MEROPE; 6 = 2.2-m Calar Alto Telescope + CAFOS; 7 = 1.82-m Copernico Telescope + AFOSC; 8 = 2.2-m ESO/MPI Telescope + WFI; H = 2-m Himalayan *Chandra* Telescope + HFOSC.

Table 7. J, H, K' magnitudes of SN 2005cf and assigned errors.

Date	JD (+240 0000)	J	H	K'	S
03/6	53525.49	14.13 (0.02)	14.13 (0.03)	14.17 (0.03)	A
16/6	53538.45	14.15 (0.03)	14.18 (0.03)	13.97 (0.03)	A
29/6	53551.48	15.59 (0.02)	14.10 (0.03)	14.26 (0.03)	B
14/7	53566.45	14.93 (0.02)	14.25 (0.03)	14.40 (0.03)	A
24/7	53576.47	15.60 (0.03)	14.75 (0.03)	15.07 (0.03)	A

Notes: A = Telescopio Nazionale Galileo 3.5 m + NICS; B = Calar Alto 3.5-m Telescope + Omega–Cass.

In Fig. 7 the $U-B$ (top left-hand panel), $B-V$ (bottom left-hand panel), $V-R$ (top right-hand panel) and $V-I$ (bottom right-hand panel) intrinsic colour curves of SN 2005cf and the other similar SNe Ia mentioned above are shown. The colour evolution of all these objects is very similar, with a few minor differences. The $U-B$ colour (Fig. 7, top left-hand panel) has a steep decline (from 0.4 to about −0.3) until ∼4 d before maximum. Then the $U-B$ colour curves become redder, arriving at ∼0.3 about 3–4 weeks past maximum and being almost constant thereafter. SNe 2001el and 2002dj have a similar evolution.

The evolution of the $B-V$ colour curves (Fig. 7, bottom left-hand panel) is very similar for all SNe of our sample, showing a

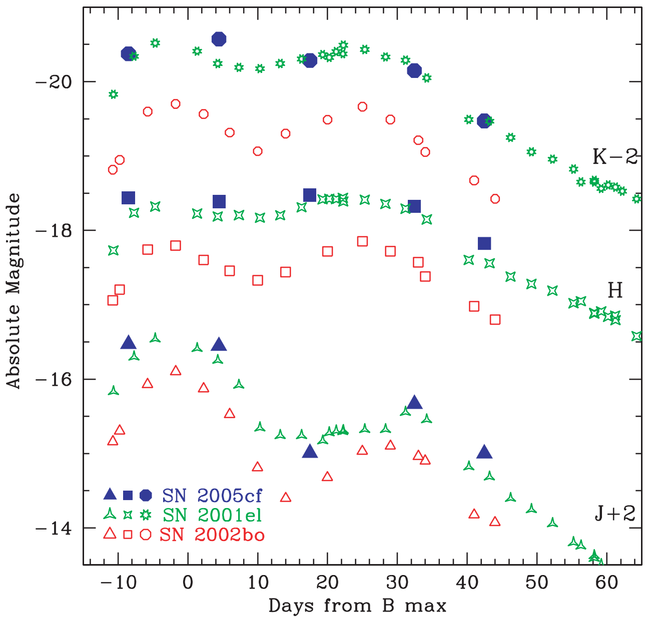

Figure 6. NIR absolute light curves of SNe 2005cf (blue filled symbols), 2001el (green starred symbols) and 2002bo (red open symbols). The sources of the data are cited in the text. K' photometry is displayed for SN 2005cf.

decreasing trend from ∼0.3 to −0.2 in the period 13–5 d before the B-band maximum. Then the $B-V$ colour rises for approximately 1 month, reaching a $B-V\approx 1.2$. In the subsequent two months, the $B-V$ colour becomes bluer again, to values below ∼0.5 at a phase of ∼90 d past maximum.

The $V-R$ and $V-I$ colours show a similar behaviour (see Fig. 7, top right-hand panel and bottom right-hand panel). Soon after the explosion, the colours turn red. Then, between about a week before and two weeks past maximum, the trend is reversed (the $V-I$ colour, in particular, decreases from 0 to −0.7 in this time interval). Subsequently, until about 1 month past the B-band maximum, the colours become again redder ($V-R$ rises from −0.2 to +0.4, $V-I$ from −0.7 to 0.6), followed by a phase where they turn bluer again. About 3 months after maximum, the $V-R$ colour reaches 0 and $V-I$ about −0.3, with an ongoing trend to bluer values in the subsequent weeks. The only outlier is SN 2002bo, which seems to have bluer $V-R$ and $V-I$ colours at all phases, especially well after maximum.

A comparison of the absolute light curves of SN 2005cf and other similar events is shown in Fig. 8, both for the B band (top panel) and the I band (bottom panel). It is remarkable that the I-band secondary maximum, known to be more or less pronounced in different SNe Ia, is similarly prominent for the SNe of this sample. The B-band maximum magnitude of SN 2005cf is $M_{B,\rm max}\approx -19.39$, which is in the bright side of the SN Ia luminosity function. At the epoch of the B-band maximum, the dereddened colour is $(B-V)_{B,\rm max}=-0.09$.

Table 8. Basic information for the SNe Ia sample with $\Delta m_{15}(B)_{\rm true}\sim 1.1$ included in this paper.

SN	Host galaxy	μ	$E(B-V)^{\otimes}_{\rm TOT}$	$\rm JD(B)_{max}$	$M_{B,\rm max}$	$\Delta m_{15}(B)_{\rm true}$	Sources
2005cf	MCG-01-39-003	32.51	0.097	245 3534.0	−19.39	1.12	1,0
2002dj	NGC 5018	32.92	0.15	245 2450.5	−19.17	1.15	2,0
2002bo	NGC 3190	31.45	0.38	245 2356.5	−18.98	1.17	3,4,0
2001el	NGC 1448	31.29	$0.22^{\ddagger}$	245 2182.5	−19.35	1.13	5
1992al	ESO 234–G069	33.82	0.034	244 8838.36	−19.37	1.11	6,0

$^{\otimes}E(B-V)_{\rm Gal}+E(B-V)_{\rm host}$; $\ddagger E(B-V)_{\rm host}=0.18$, with $R_V=2.88$.
0 = LEDA; 1 = this paper; 2 = Pignata et al. (in preparation); 3 = Benetti et al. (2004); 4 = Stehle et al. (2005); 5 = Krisciunas et al. (2003); 6 = Hamuy et al. (1996).

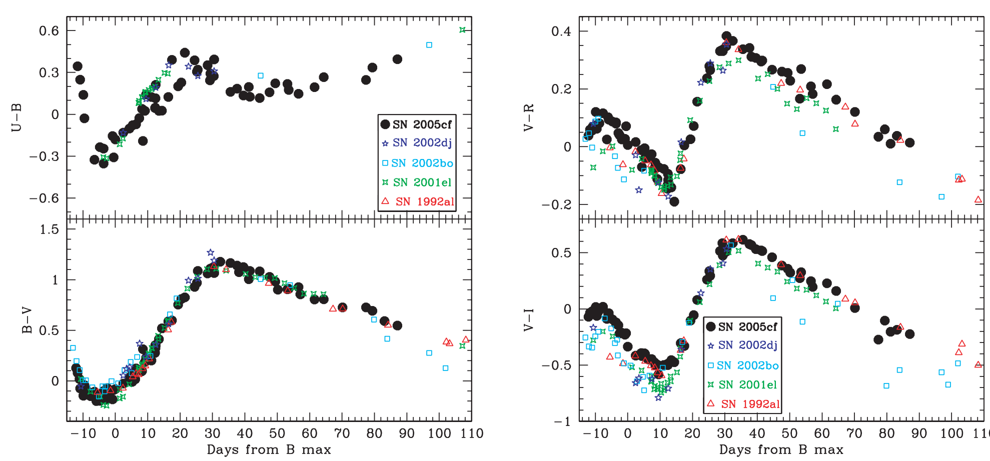

Figure 7. Colour evolution of SN 2005cf compared with other SNe Ia with similar $\Delta m_{15}(B)_{\rm true}$: SNe 1992al, 2001el, 2002bo, 2002dj. Evolution of $U-B$ (top left-hand panel), $B-V$ (bottom left-hand panel), $V-R$ (top right-hand panel) and $V-I$ (bottom right-hand panel) colours. All colour curves are reddening corrected. For references, see the text.

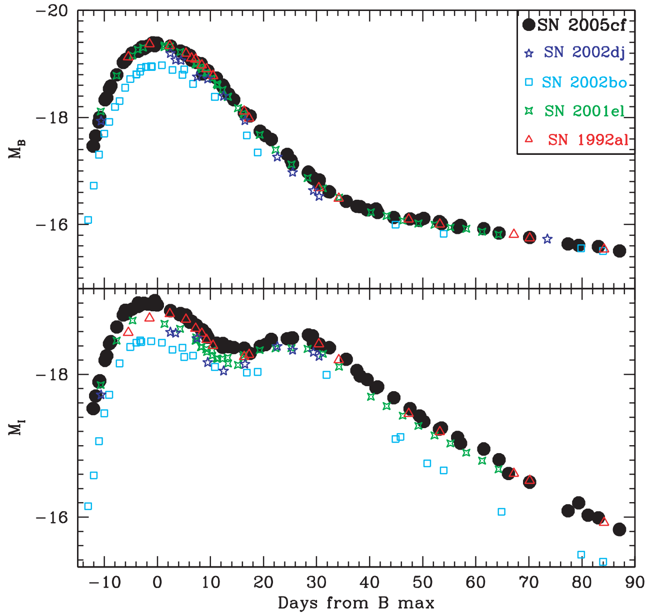

Figure 8. *B* (top) and *I*-band (bottom) absolute light curves for SN 2005cf and other similar objects: SNe 1992al, 2001el, 2002bo, 2002dj. The values of μ and $E(B-V)$ adopted are shown in Table 8.

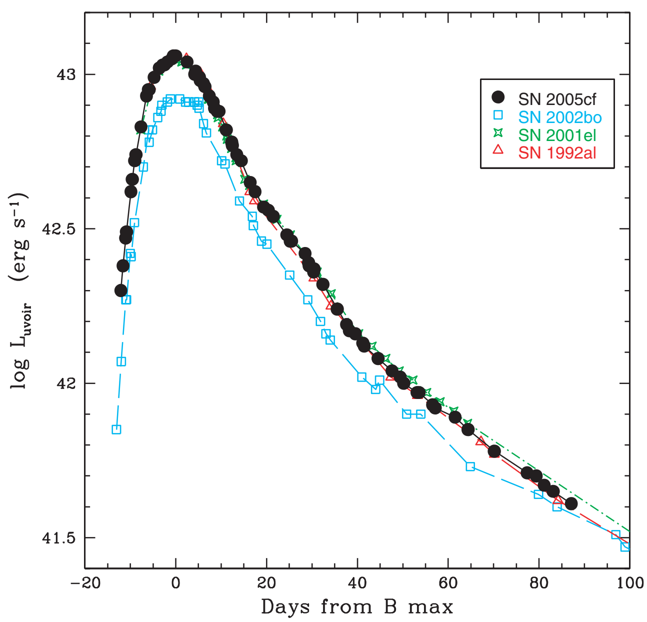

Figure 9. Quasi-bolometric light curves for SNe 2005cf, 1992al, 2001el and 2002bo. All these SNe Ia are characterized by similar values for the $\Delta m_{15}(B)$ parameter (about 1.1).

The luminosity evolution of SN 2005cf obtained integrating the fluxes in the optical bands is shown in Fig. 9. For comparison, also the observed pseudo-bolometric light curves for other similar SNe Ia are shown. Since *U*-band observations of SN 1992al are missing, we applied a *U*-band correction to its light curve following Contardo, Leibundgut & Vacca (2000). The pseudo-bolometric light curves of our Type Ia SN sample are extremely similar, with the exception of SN 2002bo, which is fainter than SN 2005cf by a factor 0.75, suggesting a non-negligible scatter in luminosity also among similarly declining SNe Ia.

Table 9. Parameters of SN 2005cf derived from the optical light curves. The errors in the absolute magnitudes are largely dominated by the uncertainty in the distance modulus estimate (±0.33). The values for A_λ are those provided by Schlegel et al. (1998).

	JD(max) (+240 00000)	$m_{\lambda,\rm max}$	A_λ	$m_{\lambda,\rm max}$	$\Delta m_{15}(\lambda)_{\rm obs}$
U	53532.4±0.6	13.40±0.05	0.53	−19.64	1.26 ± 0.05
B	53534.0±0.3	13.54±0.02	0.42	−19.39	1.11 ± 0.03
V	53535.3±0.3	13.53±0.02	0.32	−19.30	0.61 ± 0.02
R	53534.6±0.4	13.45±0.03	0.26	−19.32	0.71 ± 0.04
I	53532.0±0.5	13.70±0.03	0.19	−19.00	0.61 ± 0.06

4 SN PARAMETERS

The excellent photometric coverage of SN 2005cf allows us to precisely estimate the epoch, and the apparent and absolute magnitudes at the *B*, *V* and *I* maxima. The parameters for all bands are obtained by fitting the light curves with a low-degree spline function. The results are reported in Table 9. In particular, the epoch of the *B*-band maximum is found to be JD($B_{\rm max}$) = 245 3534.0 ± 0.3 (June 12.5 UT).

In Fig. 10 the *B*, *V* and *I* light curves of SN 2005cf are compared with those of the template SN 1992al (Hamuy et al. 1996). The match of the light curves is excellent and therefore one of the most important parameters for SNe Ia, the $\Delta m_{15}(B)$ is expected to be very similar. An observed $\Delta m_{15}(B)_{\rm obs} \approx 1.11 \pm 0.03$ is measured for SN 2005cf (see Column 6 in Table 9), well matching that derived for SN 1992al (Hamuy et al. 1996). This value makes SN 2005cf a typical SN Ia. Owing to the low interstellar extinction suffered by SN 2005cf, the correction for reddening to apply to $\Delta m_{15}(B)$ is very small. The reddening corrected $\Delta m_{15}(B)_{\rm true}$ is obtained applying the relation of Phillips et al. (1999):

$$\Delta m_{15}(B)_{\rm true} = \Delta m_{15}(B)_{\rm obs} + 0.1E(B-V). \quad (2)$$

This gives $\Delta m_{15}(B)_{\rm true} = 1.12$.

An alternative parameter characterizing the light curves of Type Ia SNe is the stretch factor s^{-1} (Perlmutter et al. 1997), that is, the coefficient indicating the stretch in time of the *B*-band light curve. We compute for SN 2005cf $s^{-1} = 0.99 \pm 0.02$. This result is in excellent agreement with the value (0.995 ± 0.179) derived applying the relation of Altavilla et al. (2004):

$$\Delta m_{15}(B)_{\rm true} = 1.98(s^{-1} - 1) + 1.13. \quad (3)$$

The $\Delta m_{15}(B)$-calibrated absolute magnitude at the *B*-band maximum can be computed applying various relations available in literature. The relation between $M_{B,\rm max}$ and $\Delta m_{15}(B)$ from Hamuy et al. (1996):

$$M^{\star}_{\lambda,\rm max} = A + B[\Delta m_{15}(B) - 1.1] \quad (4)$$

provides a preliminary tool to get a calibrated absolute magnitude at maximum for SN 2005cf. The label $M^{\star}_{\lambda,\rm max}$ is to indicate that this magnitude has to be rescaled to $H_0 = 72$ km s^{-1} Mpc^{-1}. Using the 'low extinction case' parameters reported in table 3 of Hamuy et al. (1996) and after rescaling $M^{\star}_{B,\rm max}$ to $H_0 = 72$ km s^{-1} Mpc^{-1}, we obtain $M_{B,\rm max} = -19.03 \pm 0.05$. An updated, reddening-free decline rate versus $\Delta m_{15}(B)$ relation was provided by Phillips et al.

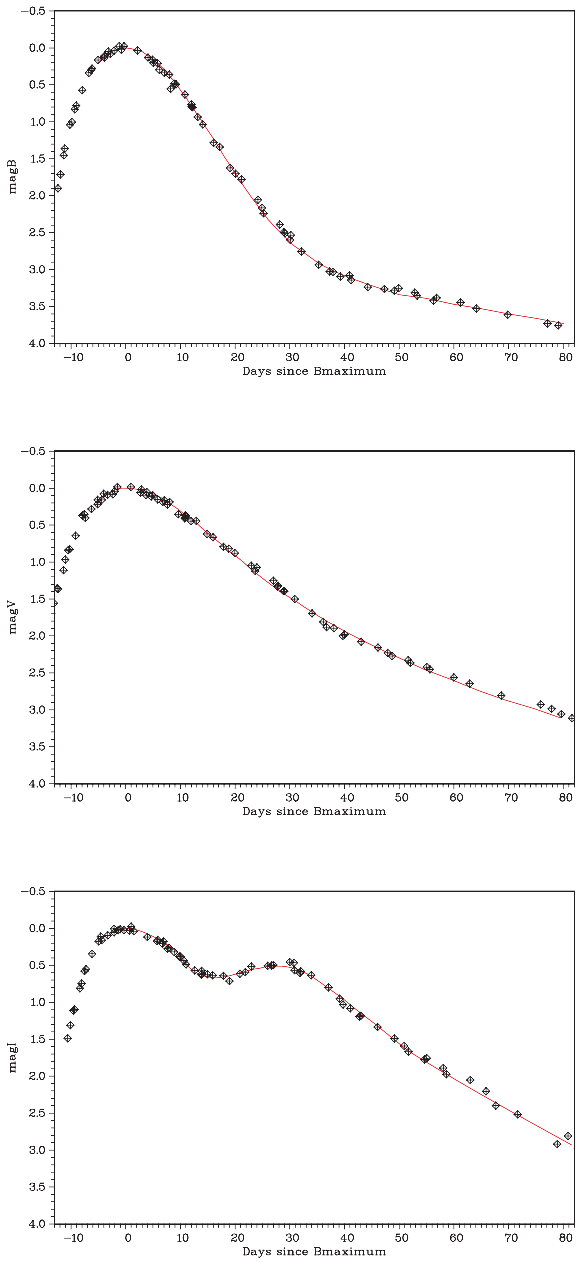

Figure 10. Comparison between light curves of SN 2005cf (diamonds) and the template SN 1992al (solid line, from Hamuy et al. 1994), in the B, V, I bands (from top to bottom).

(1999) (see also their table 3):

$$M^{\star}_{\lambda,\max} = M^{1.1}_{\lambda,\max} + a[\Delta m_{15}(B) - 1.1] + b[\Delta m_{15}(B) - 1.1]^2. \quad (5)$$

From equation (5), using as $M^{1.1}_{\lambda,\max}$ the coefficient A of equation (4) and reporting the magnitudes to $H_0 = 72$ km s^{-1} Mpc^{-1}, we derive for SN 2005cf a reddening-corrected absolute magnitude of $M_{B,\max} = 19.02 \pm 0.05$. The magnitudes for the other bands can be found in Table 10.

Altavilla et al. (2004) used a further, updated version of equation (4), with different coefficients ($A = -19.403 \pm 0.044$ and $B = 1.061 \pm 0.154$, under the assumption of intermediate Cepheids metallicity, $\Delta Y/\Delta Z = 2.5$, and with $R_B = 3.5$). Applying the relation of Altavilla et al., we obtain $M_{B,\max} = -19.35 \pm 0.06$ (for $H_0 = 72$ km s^{-1} Mpc^{-1}).

Table 10. $\Delta m_{15}(B)$-corrected absolute magnitudes for SN 2005cf. All absolute magnitudes are scaled to $H_0 = 72$ km s^{-1} Mpc^{-1}.

Method	$M_{B,\max}$	$M_{V,\max}$	$M_{I,\max}$
Phillips et al. (1999)[a]	-19.02 ± 0.05	-19.03 ± 0.05	-18.76 ± 0.05
Altavilla et al. (2006)	-19.35 ± 0.06		
Prieto et al. (2006)	-19.31 ± 0.03	-19.24 ± 0.03	-18.97 ± 0.03
Reindl et al. (2005)	-19.16 ± 0.06	-19.14 ± 0.04	-18.89 ± 0.07
Wang et al. (2005)	-19.27 ± 0.09	-19.20 ± 0.09	-18.86 ± 0.09
Average values	-19.28 ± 0.08	-19.20 ± 0.05	-18.90 ± 0.06
Distance (Table 9)	-19.39 ± 0.33	-19.30 ± 0.33	-19.00 ± 0.33

[a]Not considered in the computation of the average absolute magnitudes.

Using a large sample of SNe Ia, Prieto, Rest & Suntzeff (2006) provided an updated version of the relation between absolute B-band magnitude at peak and post-maximum decline (equation 4, but with different values for the coefficients A and B). Using the coefficients of the low host galaxy extinction case (see Prieto et al. (2006), their table 3, middle), we obtain for SN 2005cf $M_{B,\max} = -19.31 \pm 0.03$. Estimates for other bands are reported in Table 10. The discrepancy of these magnitudes with those derived from other methods (see Table 10) may be due to the uncertainty in the zero-points of the equation (4) reported in Prieto et al. (2006). Using different subsamples, the scatter in the zero-point values is between 0.10 and 0.15 magnitudes in all bands (see their table 4).

Another approach for estimating the absolute magnitude at maximum is that of Reindl et al. (2005), who computed the value from $\Delta m_{15}(B)$ and colour at maximum. Rewriting their equation (23),

$$M^{\star}_{\lambda,\max} = \alpha[\Delta m_{15}(B) - 1.1] + \beta[(B - V)_0 + 0.024] + \gamma \quad (6)$$

with the coefficients α, β and γ reported in table 5 of Reindl et al. (2005), and with $(B - V)_0$ obtained from their empirical relation

$$(B - V)_0 = 0.045\Delta m_{15}(B) - 0.073 \quad (7)$$

we obtain the absolute magnitudes shown in Table 10. For the B band it is -19.16 ± 0.06 (with $H_0 = 72$ km s^{-1} Mpc^{-1}).

An alternative method was recently proposed by Wang et al. (2005), who introduced a new parameter, the intrinsic $B - V$ colour 12 d after maximum light (ΔC_{12}), which is correlated with the absolute magnitude via the empirical formula

$$M_{\lambda,\max} = M_0 + R\Delta C_{12}, \quad (8)$$

where the parameter ΔC_{12} is found to be 0.354 ± 0.022 using $\Delta m_{15}(B) = 1.12$ and the relation of Wang et al. (2005):

$$\Delta C_{12} = 0.347 + 0.401 D^B_{15} - 0.875\left(D^B_{15}\right)^2 + 2.44\left(D^B_{15}\right)^3, \quad (9)$$

where $D^B_{15} = \Delta m_{15}(B) - 1.1$. The values of the parameters M_0 and R are reported in table 2 of Wang et al. (2005). This provides $M_{B,\max} = -19.27 \pm 0.09$. Estimates for the V and I bands are also reported in Table 10.

Averaging the calibrated absolute magnitudes obtained applying different methods (those obtained with the older relations of Phillips et al. (1999) were not considered), the following estimates have been obtained for SN 2005cf: $M_{B,\max} = -19.28 \pm 0.08$, $M_{V,\max} = -19.20 \pm 0.05$ and $M_{I,\max} = -18.90 \pm 0.06$, where the errors are the s.d. values of the available estimates (see Table 10). From the average absolute peak magnitudes, we obtain the following reddening-corrected colours: $B - V = -0.08$ and $V - I = -0.30$, which are well consistent with those obtained from the direct measurements in Table 9, being -0.09 and -0.30, respectively.

Another interesting parameter is the rise time t_r in the B band, that is, the time spent by the SN from the explosion to the B-band maximum. A first attempt to estimate this parameter was performed by Pskovskii (1984), who found it to be related to the post-maximum decay rate β, closely related to the $\Delta m_{15}(B)$, via the relation

$$t_r = 13 + 0.7\beta. \quad (10)$$

For SN 2005cf β is estimated to be about 7.47 mag/100 d, setting the explosion epoch $t_r \sim 18.2$ d before the B-band maximum. Another more recent method was suggested by Riess et al. (1999b). In a first approximation, very young SNe Ia are homologously expanding fireballs, where the luminosity is proportional to the square of time since explosion. Riess et al. (1999b) derived t_r from the relation

$$L(t) = A(t + t_r)^2, \quad (11)$$

where t is the elapsed time relative to the maximum and A is a parameter describing the raising rate. Using very early photometric data in the R band (including the earliest unfiltered measurements from IAU Circ. 8535, and considering data until ~9 d before maximum), we find that SN 2005cf exploded 19.2 d before the R-band maximum (JD = 245 3515.4). This corresponds to a rise time to maximum in the B band $t_r \approx 18.6 \pm 0.4$ d, not far from that derived applying equation (10), but slightly shorter than the 19.5 ± 0.2 d found by Riess et al. (1999b) for an object with $\Delta m_{15}(B) \approx 1.1$. However, the value of t_r obtained for SN 2005cf is in good agreement with that derived by Benetti et al. (2004) for the similar declining SN 2002bo ($t_r = 17.9 \pm 0.5$).[6]

5 LIGHT-CURVE MODELS AND ^{56}NI MASS ESTIMATE

An useful tool to estimate the properties of an SN is the modelling of its bolometric light curve. The bolometric light curves of our SN sample were computed applying the UV and NIR corrections from Suntzeff (1996) to the observed quasi-bolometric light curves of Fig. 9. The bolometric light curves of SNe 2005cf, 1992al and 2001el are identical, while that of SN 2002bo is fainter (see also Fig. 9 for a comparison). In Fig. 11 the bolometric light curves of SNe 2005cf and 2002bo (those of SNe 1992al and 2001el are not shown) are compared with the models described below. The masses of the different components of the ejecta adopted in the models are reported in Table 11.

We used a grey Monte Carlo light-curve code (Mazzali et al. 2001) to reproduce the bolometric light curve and derive the properties of the ejecta. The code computes the transport of the γ-rays and the positrons emitted by the decay ^{56}Ni $\rightarrow ^{56}$Co $\rightarrow ^{56}$Fe, and then the transport of the optical photons generated by the deposition of the energy carried by the γ-rays and the positrons in the expanding SN ejecta. We assume that the ejecta mass is 1.4 $M_\odot$, and that the density–velocity distribution is described by the W7 model (Nomoto, Thielemann & Yokoi 1984). Compared to a model with 0.7 $M_\odot$ derived with the W7 density and abundance distributions (dotted curve in Fig. 11), the light curve of SN 2005cf ($\Delta B = 1.12$, $\Delta V \sim 0.6$, Δ Bol ≈ 0.9) is broader.

A factor that could make a light curve broad for its luminosity is the relative content of (^{58}Ni+^{54}Fe)/^{56}Ni (Mazzali & Podsiadlowski 2006). For the same total mass of material in nuclear statistical equilibrium (NSE), a higher (^{58}Ni+^{54}Fe)/^{56}Ni ratio produces a dimmer light curve that has a comparable width. We find that the light curve of SN 2005cf is better fitted by models where the ratio is larger than in W7. In particular, in order to match the bolometric light curve of SN 2005cf, we start from a model where the ^{56}Ni mass is initially rescaled to 0.8 $M_\odot$, but then 10 per cent of ^{56}Ni is replaced with non-radioactive ^{58}Ni and ^{54}Fe (model Ni08–10 per cent, see Mazzali & Podsiadlowski (2006)). Such a high ratio of stable versus radioactive Fe-group elements (~50 per cent) is unlikely for W7-like ignition conditions, but is not excluded for higher ignition densities and/or higher-than-solar metallicities (Roepke at al. 2006).

The model described above (not shown in Fig. 11) has $M(^{56}$Ni) ~ 0.72 $M_\odot$ and total M(NSE) ~ 1.1 $M_\odot$ (see Table 11), but produces a luminosity peak that is too bright. In the case of SN 2002bo, the fast rise of the light curve could be reproduced adopting the ^{56}Ni distribution derived from fitting a time sequence of spectra (Fig. 11, thin lower solid curve Stehle et al. 2005). That distribution reached higher velocities than W7. In that model, $M(^{56}$Ni) ~ 0.52 $M_\odot$ and M(NSE) ~ 0.9 $M_\odot$ were adopted. Now we rescale our Ni08–10 per cent model to the abundance distribution of the model used to fit SN 2002bo, although we cannot justify this with spectroscopic results. The resulting model, with $M(^{56}$Ni) ~ 0.7 $M_\odot$ and a mass of NSE elements of about 1.1 $M_\odot$, fits the light curve of SN 2005cf quite well (Fig. 11, thick higher solid curve). In total, 1.1 $M_\odot$ are burned to NSE, and only 0.3 $M_\odot$ are intermediate-mass elements (IME) or unburned material (CO). Similar values, in particular an ejected ^{56}Ni mass of about 0.7 $M_\odot$, are also obtained for SNe 1992al and 2001el. Spectroscopic models will be necessary to refine these estimates.

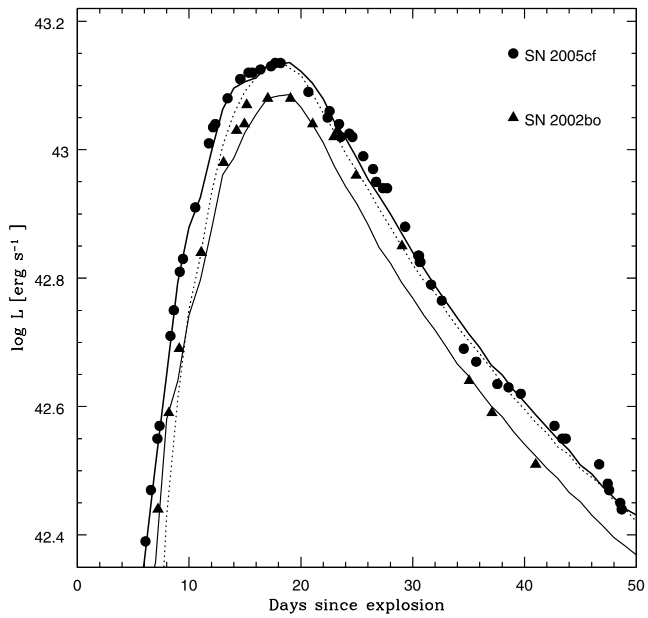

Figure 11. Comparison between the observed bolometric light curves of SNe 2005cf (circles) and 2002bo (triangles), and the bolometric light-curve models obtained using the W7 density distribution and the abundances derived from the spectral analysis of Stehle et al. (2005). The dotted curve is a W7-based model with 0.7 $M_\odot$ of ^{56}Ni. The two solid curves are a models obtained starting from Ni08–10 per cent but increasing the NSE abundances at high velocities as in Stehle et al. (2005): the thin lower curve is the model used for SN 2002bo, while the thick higher is the model rescaled to the luminosity of SN 2005cf.

[6] After submission of our paper, a preprint was posted (Conley et al. 2006) with estimates of the rise times for a sample of 73 SNe Ia. The average value for low-redshift SNe is 19.58 d, similar to the estimate of Riess et al. (1999b), and somewhat higher that our estimate for 2005cf.

Table 11. Parameters adopter in the light-curve models shown in Fig. 11.

Model	ID curve	$M(^{56}$Ni)	$M(^{58}$Ni+^{54}Fe)	M(IME + CO)
Ni07	Dotted	0.7 $M_{\odot}$	0.3 $M_{\odot}$	0.4 $M_{\odot}$
Ni08–10 per cent	‡	0.72 $M_{\odot}$	0.38 $M_{\odot}$	0.3 $M_{\odot}$
SN 2002bo	Lower solid	0.52 $M_{\odot}$	0.36 $M_{\odot}$	0.5 $M_{\odot}$
SN 2005cf	Higher solid	0.7 $M_{\odot}$	0.4 $M_{\odot}$	0.3 $M_{\odot}$

‡This model (see Mazzali & Podsiadlowski 2006) is not shown in Fig. 11.

6 SUMMARY

Extensive optical photometric observations of the nearby Type Ia SN 2005cf obtained by the ESC are presented. The observations span a period of about 100 d, from −12 until +87 d from the *B*-band maximum.

Being a standard, normally declining SN Ia, with a reddening corrected $\Delta m_{15}(B) = 1.12$, its light curves well match those of SNe 1992al and 2001el in optical bands. SN 2005cf can be considered a good template, having been discovered a short time after the explosion and being densely sampled. Despite some uncertainty in the distance of the host galaxy, its absolute magnitude at maximum ($M_B = -19.39 \pm 0.33$) is close to those of SNe 1992al and 2001el, but SN 2005cf is probably intrinsically brighter than the similarly declining SN 2002bo. The colour evolution of SNe Ia in the $\Delta m_{15}(B)$ range 1.1–1.2 appears to be rather homogeneous.

The rise time of SN 2005cf to the *B*-band maximum is computed to be 18.6 ± 0.4 d, slightly shorter than expected for an SN with such $\Delta m_{15}(B)$.

Finally, the bolometric light-curve modelling indicates an ejected^{56}Ni mass of about 0.7 $M_{\odot}$, which is close to the average value of the^{56}Ni mass distribution observed in normal SNe Ia (0.4–1.1 $M_{\odot}$, Cappellaro et al. 1997).

Spectroscopic data that will be presented in a forthcoming paper (Garavini et al., in preparation) will provide further information about the properties of this normal object, and the degree of homogeneity among the mid-declining SNe Ia.

ACKNOWLEDGMENTS

This work has been supported by the European Union's Human Potential Programme 'The Physics of Type Ia Supernovae', under contract HPRN-CT-2002-00303. AG and VS would also like to thank the Göran Gustafsson Foundation for financial support.

This paper is based on observations collected at the Centro Astronómico Hispano Alemán (Calar Alto, Spain), Siding Spring Observatory (Australia), Asiago Observatory (Italy), Telescopio Nazionale Galileo, Nordic Optical Telescope and Mercator Telescope (La Palma, Spain), ESO/MPI 2.2-m Telescope (La Silla, Chile), 2-m Himalayan *Chandra* Telescope of the Indian Astronomical Observatory (Hanle, India)

We thank the resident astronomers of the Telescopio Nazionale Galileo, the Mercator Telescope, the ESO/MPI 2.2-m Telescope and the 2.2- and 3.5-m telescopes in Calar Alto for performing the follow-up observations of SN 2005cf. We thank Thomas Augusteijn, Eija Laurikainen, Karri Muinonen and Pasi Hakala for giving up part of their time at the Nordic Optical Telescope (NOT), and Jyri Näränen, Thomas Augusteijn, Heiki Salo, Panu Muhli, Tapio Pursimo, Kalle Torstensson and Danka Parafcz for performing the observations. Observations on Aug 15 were performed by the Olesja Smirnova and Are Vidar Hansen as remote observations with the NOT at the Nordic Baltic Research School: 'Looking Inside Stars', which took place at Moletai Observatory, Lithuania, August 7-21, 2005. We are also grateful to P. Sackett for the help in observing SN 2005cf from Siding Spring.

This research has made use of the NED which is operated by the Jet Propulsion Laboratory, California Institute of Technology, under contract with the National Aeronautics and Space Administration. We also made use of the Lyon-Meudon Extragalactic Database (LEDA), supplied by the LEDA team at the Centre de Recherche Astronomique de Lyon, Observatoire de Lyon.

REFERENCES

Altavilla G. et al., 2004, MNRAS, 349, 1344
Astier P. et al., 2006, A&A, 447, 31
Benetti S. et al., 2004, MNRAS, 348, 261
Benetti S. et al., 2005, ApJ, 623, 1011
Bessell M. S., 1990, PASP, 102, 1181
Cappellaro E., Mazzali P. A., Benetti S., Danziger I. J., Turatto M., della Valle M., 1997, A&A, 328, 203
Conley A. et al., 2006, AJ, 132, 1707
Contardo G., Leibundgut B., Vacca W. D., 2000, A&A, 359, 876
Della Valle M., Livio M., 1994, ApJ, 423, L31
Della Valle M., Panagia N., Padovani P., Cappellaro E., Mannucci F., Turatto M., 2005, ApJ, 629, 750
Elias-Rosa N. et al., 2006, MNRAS, 369, 1880
Fouqué P., Solanes J. M., Sanchis T., Balkowski C., 2001, A&A, 375, 770
Garavini G. et al., 2007, A&A, in press (astro-ph/0702569)
Hamuy M., Suntzeff N. B., Heathcote S. R., Walker A. R., Gigoux P., Phillips M. M., 1994, PASP, 106, 566
Hamuy M. et al., 1996, AJ, 112, 2408
Hachinger S., Mazzali P. A., Benetti S., 2006, MNRAS, 370, 299
Hopp U., Fernàndez M., 2002, International Report 17/10/2002
Hunt L. K., Mannucci F., Testi L., Migliorini S., Stanga R. M., Baffa C., Lisi F., Vanzi L., 1998, AJ, 115, 2594
Jha S. et al., 2006, AJ, 131, 527
Kasen D., 2006, ApJ, 649, 939
King D. L., 1985, RGO/La Palma Technical Note No. 31
Kotak R. et al., 2005, A&A, 436, 1021
Kraan-Korteweg R. C., 1986, A&AS, 66, 255
Krisciunas K. et al., 2003, AJ, 125, 166
Krisciunas K. et al., 2004, AJ, 128, 3034
Landolt A. U., 1992, AJ, 104, 340
Mazzali P. A., Podsiadlowski P., 2006, MNRAS, 369, L19
Mazzali P. A., Nomoto K., Cappellaro E., Nakamura T., Umeda H., Iwamoto K., 2001, ApJ, 547, 988
Mazzali P. A. et al., 2005, ApJ, 623, 37
Modjaz M., Kirshner R., Challis P., Berlind P., 2005, IAU Circ., 8534, 3
Navasardyan H., Petrosian A. R., Turatto M., Cappellaro E., Boulesteix J., 2001, MNRAS, 328, 1181
Nomoto K., Thielemann F.-K., Yokoi K., 1984, ApJ, 286, 644
Pastorello A. et al., 2007, MNRAS, in press (astro-ph/0702565)
Perlmutter S. et al., 1997, ApJ, 483, 565

Persson S. E., Murphy D. C., Krzeminski W., Roth M., Rieke M. J., 1998, AJ, 116, 2475
Petrosian A. R., Turatto M., 1995, A&A, 297, 49
Phillips M. M., 1993, ApJ, 413, L105
Phillips M. M., Lira P., Suntzeff N. B., Schommer R. A., Hamuy M., Maza J., 1999, AJ, 118, 1766
Pignata G. et al., 2004, MNRAS, 355, 178
Prieto J. L., Rest A., Suntzeff N. B., 2006, ApJ, 647, 501
Pskovskii, Yu. P., 1984, SvA, 28, 658
Puckett T., Langoussis A., Chen Y.-T., Hu C.-P., Pugh H., Li W., Harris B., 2005, IAU Circ., 8534, 1
Reindl B., Tammann G. A., Sandage A., Saha A., 2005, ApJ, 624, 532
Riess A. G. et al., 1999a, AJ, 117, 707
Riess A. G. et al., 1999b, AJ, 118, 2675
Roepke F. K., Gieseler M., Reinecke M., Travaglio C., Hillebrandt W., 2006, A&A, 453, 203
Schlegel D. J., Finkbeiner D. P., Davis M., 1998, ApJ, 500, 525
Silk J., 1977, A&A, 59, 53
Smirnov M. A., Tsvetkov D. Yu., 1981, Pis'ma Astron. Zh., 7, 154
Somerville R. S., Davis M., Primack J. R., 1997, ApJ, 479, 616
Stanishev V. et al., 2007, A&A, submitted
Stehle M., Mazzali P. A., Benetti S., Hillebrandt W., 2005, 360, 1231
Stritzinger M. et al., 2002, AJ, 124, 2100
Stritzinger M., Suntzeff N. B., Hamuy M., Challis P., Demarco R., Germany L., Soderberg A. M., 2005, PASP, 117, 810
Suntzeff N. B., 1996, in McCray R., Wang Z., eds, Proc. IAU Colloquium 145, Supernovae and Supernova Remnants. Cambridge Univ. Press, Cambridge, p. 41
Tammann G. A., Sandage A., 1985, ApJ, 294, 81
Terry J. N., Paturel G., Ekholm T., 2002, A&A, 393, 57
Vorontsov-Velyaminov B., Arhipova V. P., 1963, Morphological Catalogue of Galaxies, Vol. 3. Moscow State University, Moscow
Walker G., 1987, Astronomical Observations. Cambridge Univ. Press, Cambridge, p. 47
Wang X., Wang L., Zhou X., Lou Y.-Q., Li Z., 2005, ApJ, 620, L87

This paper has been typeset from a TEX/LATEX file prepared by the author.